Control Engineering Practice 150 (2024) 106009

Contents lists available at ScienceDirect

Control Engineering Practice

journal homepage: www.elsevier.com/locate/conengprac

Energy-efficient trajectory planning with curve splicing based on PSO-LSTM prediction

Jian Wang [a], Zhongxing Li [a,*], Chaofeng Pan [b]

[a] School of Automotive and Traffic Engineering, Jiangsu University, Zhenjiang, 212000, China
[b] Automotive Engineering Research Institute, Jiangsu University, Zhenjiang, 212000, China

ARTICLE INFO

Keywords:
Energy-efficient trajectory planning
Curve splicing
Trajectory prediction
PSO-LSTM
RDP

ABSTRACT

Energy-efficient trajectory planning aims to optimize the economic performance for autonomous vehicles on the premise of ensuring driving safety, which excavate the energy saving potential and further improve the driving mileage. In this research, a curve splicing energy-efficient trajectory planning method based on surrounding vehicles trajectory prediction is presented. The long short-term memory (LSTM) neural network is adopted to construct the trajectory prediction model, and the hyperparameters of the LSTM are optimized by particle swarm optimization (PSO). To make the energy-efficient decision, the energy-efficient estimation model with motor MAP is developed by the correlation between vehicle driving energy consumption and motor efficiency, and the energy-efficient decision function was designed based on the average efficiency of behavior switching and the target behavior efficiency. Furthermore, a trajectory planning method with hierarchical planning of guide line and vehicle speed is presented based on B-spline curve and rolling dynamic programming (RDP). Via the traversal test, the dynamic adjustment of the guide line structure parameters is realized, and the RDP speed optimization objective function is designed with the goal of energy-efficiency. To precisely and rapidly control the EVs to track the reference trajectory, a model predictive control (MPC) with the goal of traceability was proposed. Eventually, the effectiveness of the energy-efficient trajectory planning algorithm is verified in the urban and the expressway condition respectively. The results show that the energy-efficient performance of the algorithm application is obvious in the expressway condition, and the average energy consumption improving rate is 11.11%.

1. Introduction

1.1. Background

With the increasing number and usage of vehicles, transportation has become the major field of global energy consumption. To solve this problem, the electric vehicles (EVs) are considered to be the most promising, effective and feasible solution to reduce energy consumption and pollutant emissions produced by the vehicle with internal combustion engine (ICE) (Abousleiman & Rawashdeh, 2015; Fiori et al., 2016; Miri et al., 2021). However, despite the growth of EVs market occupancy, the energy consumption performance is more important than the sustainability and environmental benefits in the customers ranking. Therefore, to improve the performance of energy consumption is a key aspect to promote the development of EVs (Luin et al., 2019; Zhao et al., 2020).

In addition, with the development of vehicle-to-infrastructure (V2I) and vehicle-to-vehicle (V2V) technologies, intelligent connected electric vehicles (ICEVs) have received a lot of attention due to the ability to optimize planning and execution of driving operations using information from the surrounding traffic and road obtained by communication and detection (Dibaei et al., 2020; Ma et al., 2021). The trajectory planning with consideration of energy consumption allows ICEVs to adjust the driving trajectory and speed to obtain energy-saving performance (Sun et al., 2020; Weißmann et al., 2018; Zhang et al., 2022). At the trajectory planning level, ICEVs are required to plan the optimal driving trajectory considering dynamics state, energy-saving performance and traffic efficiency under the premise of safety constraints comprehensively. At the control level, a tracking controller guaranteeing driving comfort and tracking is designed to make the vehicle follow the optimal trajectory. At present, the research on energy-efficient trajectory planning mainly focuses on two directions: (1) energy-efficient speed planning with ignoring the impact of lateral movement on vehicle energy consumption; (2). energy-efficient trajectory planning with considering both longitudinal and lateral movement (Li et al., 2021; Manzinger et al., 2020).

* Corresponding author.
E-mail address: zhxli@ujs.edu.cn (Z. Li).

https://doi.org/10.1016/j.conengprac.2024.106009
Received 27 February 2024; Received in revised form 21 June 2024; Accepted 21 June 2024
Available online 1 July 2024

1.2. Literature review and research gap

The most typical strategy to achieve speed optimization is the pulse glide (PnG) strategy. With this strategy, the vehicles are accelerated to high speed during the pulse phase with the efficient range of the power mechanism, and glided to low speed during the glide phase with the power mechanism closed (Tian et al., 2021). The tests have shown that PnG strategy is effective for fuel vehicles, electric vehicles and hybrid vehicles and save more than 20% in energy consumption. However, this strategy ignores the comfort constraint and has a large disturbance to the overall traffic flow and poor practicability (Shieh et al., 2023). In order to comprehensively consider safety, ride comfort and energy-efficiency, the vehicle speed planning is transformed into a multi-objective optimization problem, and the optimal acceleration and vehicle speed sequence are obtained through optimization calculation (Lin et al., 2020; Weißmann et al., 2018). He et al. proposed an improved model predictive control (IMPC) framework for plug-in hybrid EVs. This framework integrates V2V and V2I information to enhance prediction accuracy and optimize vehicle economy of speed planning (He et al., 2021). Existing researches prove that the optimization solution has improved the performance in terms of comfort and economy. In the practical design of the speed planning algorithm, the real road structure (slope, curvature and road state), signal light state and the state of the vehicle ahead are impact on the energy-efficiency performance. Therefore, Zhuang et al. proposed an economic cruising speed planning method based on approximate dynamic programming (DP), which designed a segmentation rolling form based on the distance domain. The mapping relationship between vehicle speed and road slope was established to realize the economic cruising of vehicles on different slope roads. The contribution proved that this method effectively extended the limited driving distance of EVs (Zhuang et al., 2020). In order to improve computational efficiency for eco-driving, Zhang et al. presented the speed planning method for slope driving based on iterative dynamic programming (IDP). Taking fuel economy as the optimization goal, a transient fuel consumption model was established for fuel economy evaluation, and a discrete speed planning model was developed with the vehicle dynamics equation (Zhang et al., 2022). Besides the consideration of road structure, Fei et al. designed a series of eco-approach and departure (EAD) strategies using signal phase and timing information as well as speed prediction of the vehicle ahead, which achieved optimizing speed control and energy saving (Ye et al., 2018). Lin et al. focused on the open-loop optimal control problem (OCP) formulated to minimize fuel consumption between two red-signalized intersections. This method can consider the acceleration and deceleration processes at each intersection (Lin et al., 2020). Chalaki reduced the energy consumption of vehicles at continuous intersections and adopted bi-level programming strategy (Chalaki & Malikopoulos, 2021). Under the background of prior art, vehicles obtain the distance, time and phase information of traffic lights at nearby intersections in real time, which provides time and position information reference for speed planning to make it possible to plan an energy-efficient speed. However, the eco-driving scenarios for vehicle speed planning are relatively ideal, and it is difficult to characterize random driving scenarios and microscopic traffic conditions. The speed is coupled with the trajectory in driving process and the single speed planning considering economy is difficult to meet the driving requirements of the actual scene of the vehicle.

In the random driving scenario with the time-varying traffic state, vehicles may change lanes to find more energy-efficient driving state or improve passing efficiency (Chen et al., 2019). In consequence, it is difficult to meet the requires of vehicles only by longitudinal speed planning. For the sake of further exploring the energy-efficiency potential, scholars have carried out relevant research on driving trajectory planning in different scenarios (Wang et al., 2022). According to the driving trajectory planning process, there are two main research contents: energy-efficient trajectory for keeping lane and energy-efficient trajectory for lane-changing. The method of energy-efficient trajectory for keeping lane is based on navigation data to optimize the speed, which is similar to the above for optimization of energy-efficient speed, and will not be reviewed here. Energy-efficient trajectory for lane-changing is the improvement on conventional lane-changing trajectory planning. Conventional lane changing models can be generally divided into four categories: rule-based model, discrete-choice-based model, artificial intelligence model, and incentive-based model (Rahman et al., 2013; Xie et al., 2019; Ye et al., 2018). A complete lane-changing process can be divided into three parts: lane changing decision, trajectory planning, and execution. Lane-changing decision depend on system estimation according to the traffic situation and surrounding vehicles. Subsequently, the lane-changing trajectory will be planned when the lane-changing is required. The economical optimization target is added on the existing basis to obtain the energy-efficient trajectory for lane-changing. Zhihong et al. proposed an optimal lane-changing trajectory planning model for autonomous vehicles. which was modeled as an optimal control problem with minimum energy consumption. In order to simplify the optimal control model, the speed and acceleration were decomposed in X and Y directions to transform nonlinear constraints of the optimal control into linear constraints (Yao et al., 2023). Liang et al. proposed a novel online motion planning method for marine vehicles, which can take practical limitations into account and make tradeoffs between the two objectives by exploiting the economic model predictive control (EMPC) technique. The results of tests have shown that the effectiveness and feasibility of the proposed method are validated (Liang et al., 2022). Based on the NGSIM database and the polynomial trajectory curve, it was verified that the optimal lane-changing trajectory could significantly reduce the energy consumption. In Min et al. (2023), an energy-saving driving model is established based on the proximity policy optimization (PPO) reinforcement learning method, which combined driving intention prediction and lane-change time prediction to improve the prediction accuracy of surrounding vehicle trajectories. The model takes the current state and predicted trajectories of surrounding vehicles as input information, and outputs energy saving control variables while considering various constraints such as safety, comfort, and driving efficiency. Zifei et al. proposed a novel personalized lane-changing trajectory planning strategy for energy-saving autonomous driving. A quintic polynomial is used as a general trajectory clustering generator, and the overall trajectory planning is transformed into a constrained optimization problem, and energy-efficient lane-changing trajectories are extracted from general trajectory clusters by introducing a stable handling envelope and a safe lane-changing region considering vehicle dynamics constraints (Nie & Farzaneh, 2023). In addition, scholars have carried out extensive research on trajectory planning without energy consumption evaluation. Liu et al. presented a typical lane-changing trajectory planning method with the consideration of preceding and lagging vehicles, which equipped a dynamic decoupling model to solve the problems of real-time application to provide viable solutions. The results highlighted that the proposed method can generate a satisfactory lane-changing trajectory for automatic lane-changing actions (Liu et al., 2021). Werling et al. proposed a trajectory planning algorithm based on the optimal control of on-road driving in the presence of dynamic and static obstacles. The polynomial curve is commonly exploited to generate decision trajectories (Werling et al., 2010). Wang et al. developed a trajectory planning method for lane-changing, in which the quintic function is exploited to link the initial position with the final position of the ego vehicle (Wang & Wei, 2020). However, the lane-changing trajectory planning methods mentioned above only consider the instantaneous traffic state and are difficult to cope with the dynamic driving conditions.

To sum up, most of the energy-efficiency problems of vehicle driving, in the existing researches, focus on economic speed planning with reducing energy consumption as the objective function. Combining different scenarios and algorithms have achieved certain results.

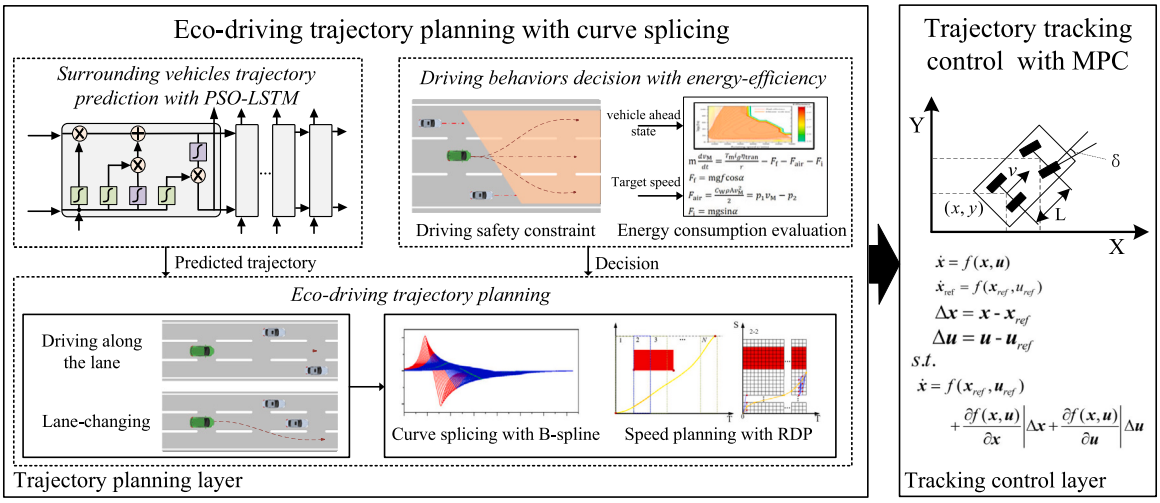

Fig. 1. System architecture of the Energy-efficient trajectory planning.

However, there are few studies that consider energy-efficiency in microscopic vehicle driving trajectories planning. The existing researches on trajectory planning mainly involved driving safety, comfort, and algorithm design and optimization combined with specific scenarios. Furthermore, the optimization problem of energy efficiency under the premise of ensuring driving safety needs to be studied, which can more accurately optimize the trajectory of the actual driving trajectories with the goal of energy-efficiency to improve the energy-efficiency and extend the driving range of the vehicle.

1.3. Contribution and novelty

Energy optimization in the decision-making and planning process of autonomous driving vehicles is an urgent problem to be solved. This paper proposes a curve splicing energy-efficient trajectory planning method based on PSO-LSTM motion prediction for automatic EV. In the unmanned driving environment, the vehicle can obtain the real-time motion state of the surrounding vehicles through the on-vehicle radar, camera and V2V technology. Because the vehicle motion is based on certain rules and has certain timing characteristics, the LSTM is used to construct the prediction model for surrounding vehicle motion trajectory. Most of the existing studies optimize the network structure by manually adjusting the LSTM hyperparameters, which is random and inaccurate. To solve this problem, this paper combines the PSO optimization algorithm to automatically adjust the LSTM hyperparameters and find the optimal hyperparameters to improve the accuracy of the trajectory prediction model. Since vehicle speed is the factor that has a great influence on energy consumption in the planning process, the hierarchical planning method is used to decouple the guide line and vehicle speed. In addition, the energy saving evaluation of potential behaviors is added to the vehicle decision-making process, which further improves the exploitation of energy saving potential.

1.4. System architecture

To realize the energy-efficient trajectory planning, the overall system can be designed into energy-efficient trajectory planning layer and trajectory tracking control layer, as illustrated in Fig. 1. The trajectory planning layer consists of three steps: (i) PSO-LSTM is used to predict the driving trajectory of surrounding vehicles to represent the obstacles in the potential driving trajectory of the host vehicle in the coming time; (ii) On the premise of safe driving, the potential behavior of the host vehicle is evaluated for energy-efficiency to make decision; (iii) Curve splicing with B-spline and rolling dynamic programming (RDP) are adopted to plan the driving guide line and speed. In order to ensure the vehicle's tracking for the planned trajectory, the MPC is used to design tracking algorithms.

1.5. Paper organization

The remainder of this paper is organized as follows. In Section 2, combined with PSO optimization and LSTM network, the surrounding vehicle trajectory prediction model is constructed based on the public dataset. In Section 3, through the analysis of energy saving potential in the decision-making and trajectory planning process, the energy-efficient decision-making and the energy-efficient trajectory planning based on trajectory splicing are designed. The trajectory tracking controller is designed based on MPC control theory in Section 4. Finally, the EV equipped with the proposed algorithm are tested and discussed, respectively, based on hardware in the loop (HiL) under the urban and expressway conditions in Section 6.

2. Vehicle trajectory prediction with PSO-LSTM

Surrounding vehicles trajectory will directly affect the planning of the host vehicle's potential motion, especially when sudden acceleration, deceleration and steering occur. Furthermore, the coming trajectory sequence of surrounding vehicles can be used as constraint for host vehicle planning, which can improve the accuracy of decision-making process and the safety of vehicle driving (Huang et al., 2022; Wang et al., 2021).

Trajectory prediction is one of the temporal prediction problems, which can be modeling by neural network. LSTM network effectively solves the problem that traditional neural network is prone to local minimization, gradient disappearance and explosion. At the same time, it has strong modeling and analysis ability for time series data. Conventional temporal prediction requires manual adjustment of network hyperparameters to obtain suitable network structure. The adjustment process of this method is complicated and can only get approximately optimal hyperparameters. Existing studies have discussed the setting of LSTM network related hyperparameters, and the results have shown that the main hyperparameters affecting the accuracy of the network are learning rate and network size (number of layers). Particle swarm optimization (PSO) is considered as a method to solve multi-element optimizing problems. In the whole process, the particles pass their information to each other, and the information of the current optimal

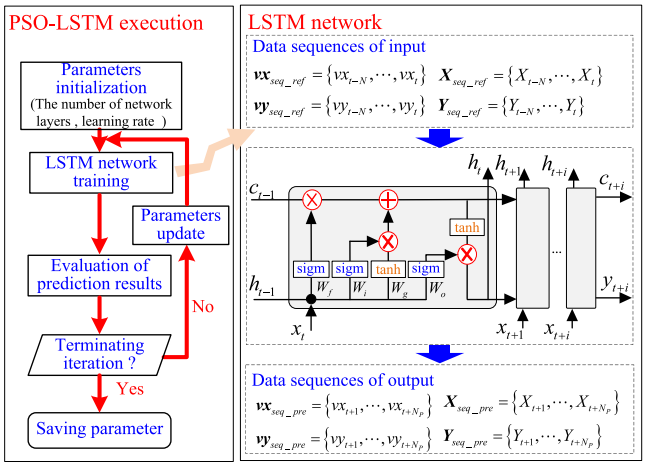

Fig. 2. Execution flow and network structure of PSO-LSTM.

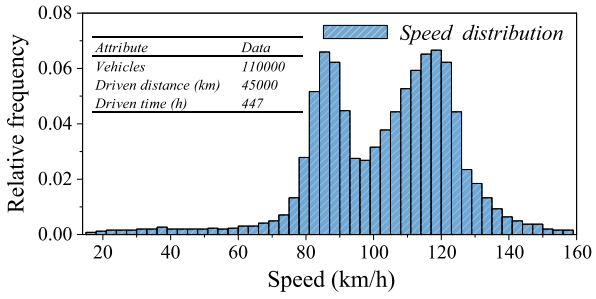

Fig. 3. The distribution of the dataset according to vehicle speed.

solution is also passed to the whole particle swarm. Finally, the whole particle swarm can converge to the optimal solution. Therefore, to improve the accuracy of modeling, this research utilizes PSO algorithm to dynamically optimize LSTM hyperparameters.

2.1. Modeling of PSO-LSTM trajectory prediction

PSO algorithm is used to optimize the number of network layers and learning rate for LSTM to obtain the optimal network structure as Fig. 2. In order to provide sufficient training and test data, HighD dataset is used to extract vehicle driving trajectory to construct the training and test data (Krajewski et al., 2018). The distribution of the HighD dataset according to vehicle speed is shown in Fig. 3, mainly concentrated in the middle and high speed interval. A total of 110,000 vehicles participated in the test, with a total test mileage of 45,000 km and a test time of 447 h. The applicable range of the network training based on this dataset corresponds to the vehicle speed distribution interval of the dataset. Equivalent to the actual road mainly for the urban condition with middle speed and expressway. Through the preliminary research, the space of energy-efficiency planning is mainly for the middle and high speed interval, so this paper uses the HighD dataset as the research object.

Furthermore, the LSTM model is established, which mainly consists of two parts: the storage unit for summarizing the historical input and storing the information, and the gating mechanism for controlling the related gate output state and updating the memory information. The input data sequences of the algorithm are longitudinal coordinate reference sequence, $\boldsymbol{X}_{seq\_ref}$, lateral coordinate reference sequence, $\boldsymbol{Y}_{seq\_ref}$, longitudinal vehicle speed reference sequence, $\boldsymbol{vx}_{seq\_ref}$, lateral vehicle speed reference sequence, $\boldsymbol{vy}_{seq\_ref}$; and the output data

Table 1
LSTM equations and structure parameters.

LSTM equations	
Input gate controller	$i_t = \mathrm{sigm}(W_{x,i}x_t + W_{h,i}h_{t-1} + b_i)$
Forget gate controller	$f_t = \mathrm{sigm}(W_{x,f}x_t + W_{h,f}h_{t-1} + b_f)$
Output gate controller	$o_t = \mathrm{sigm}(W_{x,o}x_t + W_{h,o}h_{t-1} + b_o)$
Activation function	$g_t = \tanh(W_{x,g}x_t + W_{h,g}h_{t-1} + b_g)$
Cell memory	$c_t = f_t \otimes c_{t-1} + i_t \otimes g_t$
Output	$y_t = h_t = o_t \otimes \tanh(c_t)$
Network structure parameters	
Input layer	4
LSTM layer	LL_{PSO}
Fully connected layer	4
Output layer	Regression
Learn rate	LR_{PSO}

sequences of the algorithm are longitudinal coordinate predicted sequence, $\boldsymbol{X}_{seq\_pre}$, lateral coordinate predicted sequence, $\boldsymbol{Y}_{seq\_pre}$, longitudinal vehicle speed predicted sequence, $\boldsymbol{vx}_{seq\_pre}$, lateral vehicle speed predicted sequence, $\boldsymbol{vy}_{seq\_pre}$. The relevant equations for the memory unit and the gating mechanism are described as Table 1. N is the length of reference sequence, N_{pre} is the length of predicted sequence, sigm and tanh stand for sigmoid and tangent function, x_t and y_t represent the current input and output, $W_{x,i}$, $W_{h,i}$, $W_{x,f}$, $W_{h,f}$, $W_{x,o}$, $W_{h,o}$, $W_{x,g}$ and $W_{h,g}$ are the linear transition matrixes, b_i, b_f, b_o and b_g are offset vectors, i_t, f_t and o_t are gate vectors, c_t and h_t are cell storage memory vectors, and LL_{PSO} and LR_{PSO} are optimized hyperparameters obtained by PSO optimization.

2.2. Construction of PSO optimization problem

The training of PSO-LSTM network is divided into two parts: hyperparameters optimization and model training. The optimizing the number of layers and the learning rate for LSTM by PSO is shown in Fig. 4. The PSO is initialized into a group of random particles (random solutions). Then the optimal solution is found through iteration. In each iteration, the particle is updated by tracking the two current optimal values. The particle velocity update consists of three parts. The first part is the inertia of the particle as it maintains its previous speed, which represents "memory". The second part is the understanding of the particle itself. The third part is the information exchange and cooperation between particles, which is manifested as "socialization". The particle uses Eqs. (1) and (2) to update its speed and position for the next iteration.

$$V_{id}^{n+1} = w \cdot V_{id}^{n} + c_1 \cdot r_1 \cdot (Pb_{id}^{n} - L_{id}^{n}) + c_2 \cdot r_2 \cdot (Pg_{d}^{n} - L_{id}^{n}) \tag{1}$$

$$L_{id}^{n+1} = L_{id}^{n} + V_{id}^{n+1} \tag{2}$$

where V_{id}^{n+1} and L_{id}^{n+1} represent the speed and position of the n+1th iteration of the ith particle in d dimension space, Pb_{id}^{n} is the best position searched by the ith particle at the nth iteration in d dimension, Pg_{d}^{n} is the best position searched by the global particle swarm at the nth iteration. w is the inertia weight, c_1 and c_2 represent the weight coefficients of Pb_{id}^{n} and Pg_{d}^{n}, respectively, r_1 and r_2 represent random distribution coefficients. The space used to optimize the LSTM network structure is a 2-dimensional space composed of the number of network layers and the learning rate. Each particle historical best position and the global best position are updated in each iteration as follows:

$$Pb_{id}^{n+1} = \begin{cases} L_{id}^{n+1}, & f(L_{id}^{n+1}) \le f(Pb_{id}^{n}) \\ Pb_{id}^{n}, & f(L_{id}^{n+1}) > f(Pb_{id}^{n}) \end{cases} \tag{3}$$

$$Pg_{d}^{n+1} = \begin{cases} Pg_{d}^{n}, & f(Pg_{d}^{n}) \le \min_i(f(Pb_{id}^{n+1})) \\ Pb_{id}^{n+1}, & f(Pg_{d}^{n}) > \min_i(f(Pb_{id}^{n+1})) \end{cases} \tag{4}$$

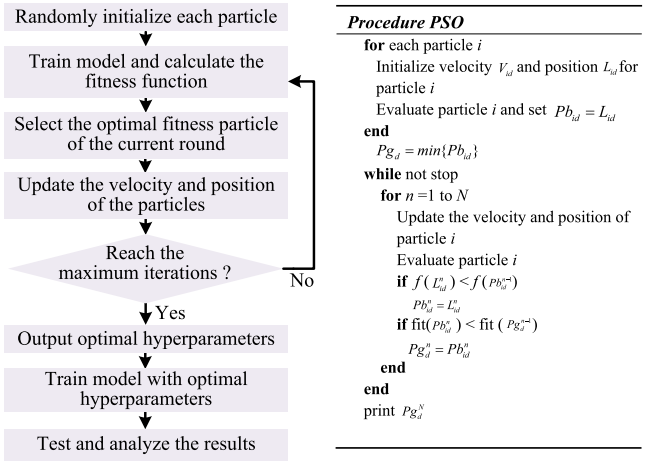

Fig. 4. The process of PSO optimizing for the hyperparameters.

The update goal is to make the prediction error smaller, and objective function is defined as:

$$f = \frac{1}{4}\sqrt{\frac{1}{N_{pre}}\sum_{1}^{N_{pre}}(\boldsymbol{X}_{seq\_ref} - \boldsymbol{X}_{seq\_pre})} + \frac{1}{4}\sqrt{\frac{1}{N_{pre}}\sum_{1}^{N_{pre}}(\boldsymbol{Y}_{seq\_ref} - \boldsymbol{Y}_{seq\_pre})} + \frac{1}{4}\sqrt{\frac{1}{N_{pre}}\sum_{1}^{N_{pre}}(\boldsymbol{vx}_{seq\_ref} - \boldsymbol{vx}_{seq\_pre})} + \frac{1}{4}\sqrt{\frac{1}{N_{pre}}\sum_{1}^{N_{pre}}(\boldsymbol{vy}_{seq\_ref} - \boldsymbol{vy}_{seq\_pre})} \tag{5}$$

The specific operation steps of PSO-LSTM are as follows:

*Step*1: The trajectory data are normalized to [−1,1] using the *mapminmax* function, and the processed data is divided into training sets and test sets.

*Step*2: PSO algorithm assigns current network layer number and learning rate to LSTM for constructing the network.

*Step*3: The current network is training and tested, and the current objective function value is computed. Next, by comparing the current and last objective function value, the smaller is obtained to update the global optimum.

*Step*4: According to Eqs. (1) and (2) to update the speed and position, the new network structure hyperparameters are determined. The current network structure with updated hyperparameters is trained and tested. After that, return to Step3 to evaluate the network until the global optimum is no longer updated.

*Step*5: The optimal network structure is determined and the final evaluation is carried out.

2.3. Results analysis of prediction algorithm

The network structure under different network layers and learning rate was trained and tested to verify the effectiveness of PSO-LSTM. The sampling frequency of the data was 25 Hz, and the prediction time domain was N_p=25, that is, the trajectory in the future one second is predicted. Case1-4 is the traditional parameter configuration of LSTM, which relatively good parameter configuration is obtained by manual adjustment based on experience in the existing literatures. Case 5 is the hyperparameters setting of the PSO-LSTM network, which replaces the manual parameter tuning process by PSO iterative optimization. The specific parameters are shown in Table 2, and test results are shown in Figs. 5, 6 and 7. The Average RMSE of prediction with different network structures is in Table 3.

The validity of the prediction model is experimented by selecting the vehicle driving data that is not used for model training and testing.

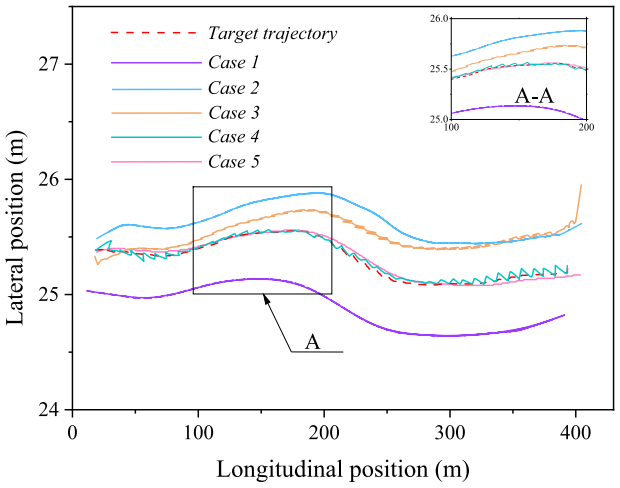

Fig. 5. Position (X, Y) prediction results with different.

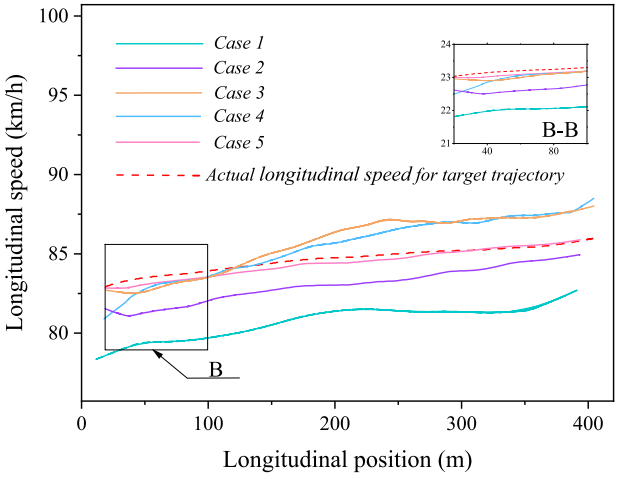

Fig. 6. Longitudinal speed (X, vx) prediction results with different network structures.

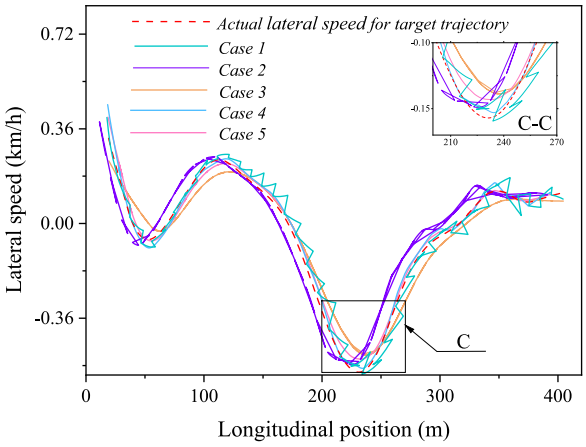

Fig. 7. Lateral speed (X, vy) prediction results with different network structures.

Table 2
Network hyperparameters for LSTM and PSO-LSTM.

Hyperparameters setting		LSTM layer	Learn rate
LSTM	Case 1	150	0.01
	Case 2	150	0.001
	Case 3	300	0.01
	Case 4	300	0.001
PSO-LSTM	Case 5	289	0.0042

Table 3
Average RMSE of prediction with different network structures.

Hyperparameters setting		Average RMSE		
		(X,Y)	(X,vx)	(X,vy)
LSTM	Case 1	9.4691	0.6832	0.0027
	Case 2	3.7041	0.3022	0.0018
	Case 3	2.1964	0.4455	0.0035
	Case 4	1.6647	0.2335	0.0024
PSO-LSTM	Case 5	9.4691	0.2168	0.0028

As can be seen from the results, the selection of network structure hyperparameters has a great impact on the prediction results. When the network structure has the same LSTM layer, the learning rate directly affects the network's ability to learn data features and the final result. According to the setting of LSTM network hyperparameters, the control variable method is used to compare the prediction results under different network layers and learning rate. The analysis of the prediction results shows that the two variables are not simple linear correlation. Specifically, comparing case 1 and 2, the increase of the learning rate can bring the prediction results closer to the reference value to some extent. However, predicted results have fluctuated back and forth from case 3 and 4, which is overfit due to the increase in learning rate. The predicted results of PSO-LSTM are shown in case 5, and the predicted trajectory is relatively smooth. As shown in Table 3, the Average RMSE of the position prediction is 0.2637, which is the minimum value among the 5 cases. The Average RMSE of longitudinal and lateral speed prediction results is 0.2168 and 0.0028, which are also the minimum values in the 5 cases. The results verify the effectiveness of PSO-LSTM network structure for trajectory and speed prediction.

3. Energy-efficient trajectory planning with curve splicing

Design curve splicing trajectory planning method includes two parts: energy-efficient driving decision-making and trajectory splicing method. The purpose of energy-efficient driving decision-making is to make economic decisions on vehicle driving behavior (cruising, following and lane changing) according to the current vehicle environment and vehicle state. The trajectory splicing method is to construct the driving trajectory of the vehicle based on the decision result.

3.1. Design of energy-efficient driving decision-making

The decision-making process is divided into two parts: safety decision-making that has a high priority and energy-efficient decision-making. That is, energy-efficient driving decision-making is carried out under the premise of ensuring safety.

3.1.1. Safety decision-making based on driving behaviors

In order to make effective safety decision-making, distance between the host vehicle and the surrounding vehicles is established. The distance for typical driving behaviors between the host vehicle and surrounding vehicles is shown in Fig. 8. The minimum longitudinal safety distance of critical collision is calculated by the quadratic integral of the speed between the vehicle and the potential collision vehicle in

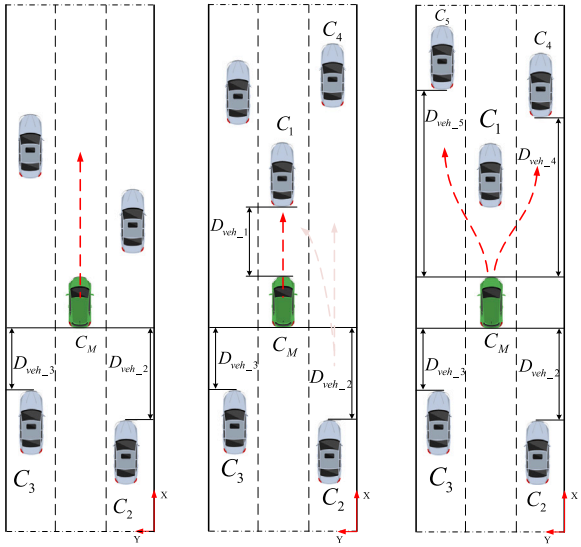

(a) Cruising behavior (b) Following behavior (c) Lane-changing behavior

Fig. 8. The distance for typical driving behaviors between host vehicle and surrounding vehicles.

combination with the initial speed difference, satisfying the following expression:

$$MSS(C_M, C_i) = \max\left\{ \int_0^t \int_0^\lambda [a_M(\tau) - a_i(\tau)]d\tau d\lambda + [v_M(0) - v_i(0)]t \right\}, \forall t \in [0, t_{thr}] \tag{6}$$

s.t.

$$t_{thr} = \begin{cases} t_c, & \text{Following} \\ t_f, & \text{Lane} - \text{changing} \end{cases} \tag{7}$$

where C_M and C_i (i=1,2,3…) represent host vehicle and surrounding vehicles, D_{veh_i} (i=1,2,3…) is the actual longitudinal distance under the target behavior, a_M and v_M are the acceleration and speed of host vehicle, a_i (i=1,2,3…) is the accelerations of C_i, v_i (i=1,2,3…) is the speeds of C_i, t_c is the collision time, t_f is the required time of lane-changing, which is experimented by actual vehicle testing.

Based on the critical minimum longitudinal safety distance and combined with the vehicle execution response time, the longitudinal safety distance model is established as:

$$d_{s,i} = \begin{cases} MSS(C_M, C_i) & , v_M < v_f \\ (v_M - v_f)t_{ttc} + MSS(C_M, C_i) & , v_M \geq v_f \end{cases} \tag{8}$$

where v_f is the speed of target vehicle, and t_{ttc} is the time of vehicle execution response. The safety decision function is constructed as follows:

$$DEC_{sef} = \begin{cases} NO\_SEF & , D_{veh\_i} < d_{s,i} \\ YES\_SEF & , D_{veh\_i} \geq d_{s,i} \end{cases} \tag{9}$$

where DEC_{sef} represents the safety decision function, NO_SEF and YES_SEF indicate that the potential behaviors dissatisfy and satisfy the safety. This function can initially determine the potential safety behavior and prepare the foundation for the energy-efficient decision-making.

3.1.2. Energy-efficient decision-making based on motor MAP

To realize the energy-efficient decision-making of the vehicle during driving state, firstly, the method of energy-efficient evaluation should

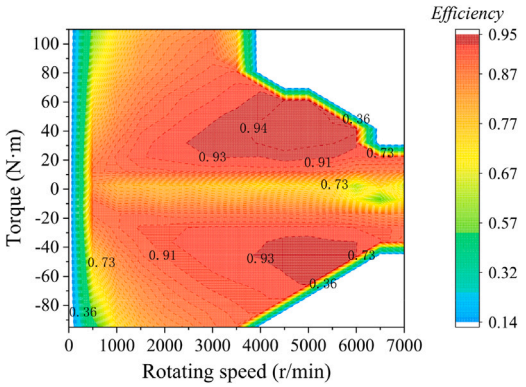

Fig. 9. The MAP of motor efficiency.

be constructed. The most direct method is the total driving energy consumption of vehicles in a period of time or a certain distance. However, that is a result evaluation for the process, which is difficult to apply to instantaneous decision-making. Inspired by this, to transform process evaluation into state evaluation, vehicle energy saving performance is evaluated through vehicle driving efficiency. There are two main systems to cause energy loss during driving: powertrain system and motor. The transfer efficiency of powertrain system is shown as follows:

$$\eta_{tran} = \frac{r}{T_{mot} i_g i_0}\left(m_M g f \cos\alpha + \frac{C_W \rho_a A v_M^2}{2} + m_M g \sin\alpha + \delta_{rq} m_M \frac{dv_M}{dt}\right) \tag{10}$$

where η_{tran} is the transfer efficiency of powertrain system, m_M is the vehicle mass, T_{mot} is the motor output torque, i_g and i_0 are the transmission ratio of the gearbox and the main reducer, r is the wheel radius, g is the acceleration of gravity, f is the rolling resistance coefficient, α is the road slope, C_W is the wind resistance coefficient, ρ_a is the air density, A is the upwind area and δ_{rq} is the rotational mass conversion coefficient. The commonly motor efficiency evaluation can be approximated by the motor equation, but with low accuracy. To further improve the precision of decision-making, this research obtains the motor efficiency of each operating point through experiments, and builds the MAP as shown in Fig. 9.

According to the transfer equation of the vehicle powertrain system, the vehicle state can be converted to the motor rotating speed and torque. By lookup on the MAP as following, the motor efficiency is obtained under the current working condition:

$$\eta_{mot} = Interp\_MAP(N_{mot}, T_{mot}) \tag{11}$$

$$N_{mot} = \lambda_{unit} \frac{v_M i_g i_0}{r} \tag{12}$$

$$T_{mot} = F(a_M, v_M) \tag{13}$$

where η_{mot} is the motor efficiency, $Interp\_MAP$ is the MAP interpolation function, N_{mot} is the motor speed, T_{mot} is motor torque, λ_{unit} is unit conversion factor, and $F(\cdot)$ is the torque calculating function which depend on the target vehicle powertrain.

In order to accurately evaluate energy-efficiency, the evaluated objective is divided into two parts, which are the efficiency of driving behavior switching and switch completion which depends on the target behavior. The speed change between the current speed and the corresponding speed of switch completion is discretized. The average motor efficiency of the process is calculated as the efficiency of driving behavior switching, and the motor efficiency of target behavior starting is calculated as the efficiency of switch completion. The calculation is as following:

$$\eta_{mot\_ave} = \frac{1}{N_{end}} \sum_{t=0}^{t_{end}} \left\{ Interp\_MAP\left[\lambda_{unit} \frac{v_M^t i_g i_0}{r}, F(a_{exp,M}^t, v_M^t)\right]\right\} \tag{14}$$

$$\eta_{mot\_tar} = Interp\_MAP\left[\lambda_{unit} \frac{v_M^t i_g i_0}{r}, F\left(\frac{v_i^2 - v_M^2}{2D_{veh\_i}}, v_M\right)\right] \tag{15}$$

where η_{mot_ave} is the average motor efficiency, η_{mot_tar} is the motor efficiency of target behavior starting, v_M^t is the instantaneous speed of the host vehicle, which is calculated by the expected acceleration at the last moment, t_{end} is the time of the behavior switching which is discrete into N_{end} time steps. The expected acceleration $a_{exp,M}^t$ is calculated using Shinichi UCHIYAMA's fast response theory, which regards the vehicle acceleration process as a damping process, which is related to the mass of the vehicle. The calculation is as follows:

$$a_{exp,M}^t = \min\left\{\frac{1}{m_M}\left[k_d(d_{s,i} - D_{veh,i}^t) + c_v(v_i - v_M^t)\right], a_{\max}\right\} \tag{16}$$

$$c_v = 2\varphi_{res}\sqrt{m_M k_d} \tag{17}$$

where k_d is the virtual stiffness coefficient, c_v is the virtual damping coefficient, $a_{exp,M}^t$ is the expected acceleration during driving behaviors witching, and φ_{res} is the vehicle response coefficient, which is related to the vehicle type. The vehicle acceleration process is similar to one degree of freedom vibration system, and the value of φ_{res} is generally 0.7.

Therefore, the energy-efficient decision-making is constructed as follows:

$$DEC_{eco} = \begin{cases} NO\_ECO, w_{eco1}\eta_{mot\_ave} + w_{eco2}\eta_{mot\_tar} < \eta_{thr} \\ YES\_ECO, w_{eco1}\eta_{mot\_ave} + w_{eco2}\eta_{mot\_tar} \geq \eta_{thr} \end{cases} \tag{18}$$

where DEC_{eco} is the energy-efficient decision-making function, w_{eco1} and w_{eco2}, are the energy-efficient weight coefficients, and η_{thr} is the efficiency threshold which is related to current vehicle state.

3.2. Design of energy-efficient trajectory planning algorithm

3.2.1. Guide line planning with B-spline curve

When the vehicle is driving as lane-keeping, the guide is the lane center line, which can be obtained by V2I or navigation information. When the vehicle is lane-changing, the guide line is obtained by geometric curve planning. Since the actual driving is to realize the curve tracking through the steering system, the wheel angle must change continuously without saltation. Moreover, to splice the trajectory between lane center line and lane-changing guide line, the curvature of the starting point of lane-changing guide line is required to be 0 m^{-1}. That ensures the switching between lane-keeping and lane-changing.

The results of geometric parameters of different geometric curves in the same lane-changing scene are compared as Figs. 10 and 11.

The four types of lane-changing guide lines have the characteristics of similar geometric structure, but the curvature of each curve is quite different. The curvature of Dubins curve is equipped with saltation, which requires step-input in the steering system during lane-changing, but that process does not satisfy the input characteristics of the steering system. The curvature of Sine curve and Bessel curve meet the requirement of continuous changing, but the curvature is not 0 at the

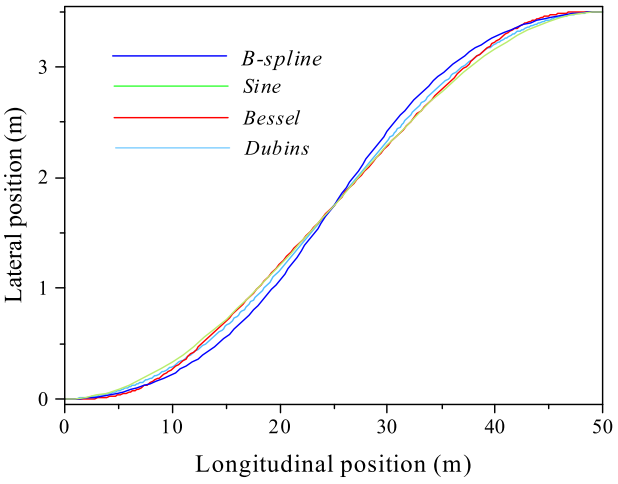

Fig. 10. Lane-changing guide line with different geometric curves.

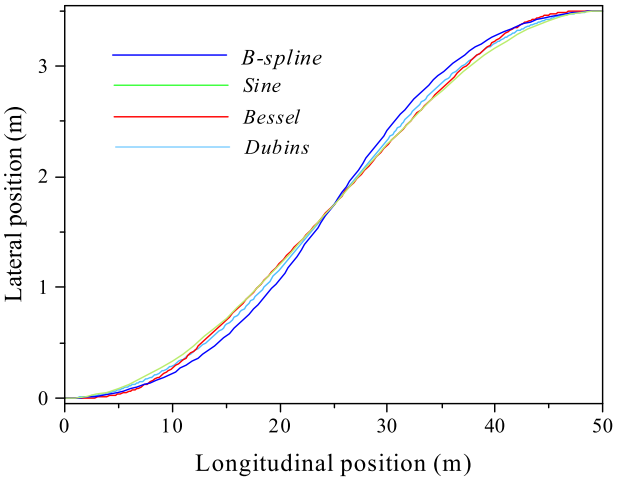

Fig. 11. Curvature of Lane-changing guide line with geometric curve.

starting point and the ending point of the lane-changing guide line. With generalized analysis, B-spline curve can avoid the defects of other curves. B-spline curve of k-order is defined as:

$$P(u) = [P_0 \cdot P_1 \cdots P_n] \begin{bmatrix} B_{0,k}(u) \\ B_{1,k}(u) \\ \vdots \\ B_{n,k}(u) \end{bmatrix} = \sum_{i=0}^{n} P_i B_{i,k}(u) \tag{19}$$

where P_n is the control point, $B_{n,k}(u)$ is the B-spline basis function of k-order, and u is the vector. Each control point corresponds to a basis function, and the recursion formula of the basis function is the Cox-De Boor recursion equation, as shown below:

$$B_{i,k}(u) = \begin{cases} \begin{cases} 1, & u_i \le u < u_{i+1} \\ 0, & others, \end{cases} & k = 1 \\ \frac{u-u_i}{u_{i+k-1}-u_i} B_{i,k-1}(u) + \frac{u_{i+k}-u}{u_{i+k}-u_{i+1}}, & k \ge 2 \end{cases} \tag{20}$$

In the formula, for the convenience of calculation, 0/0=0 is agreed. According to the recursion, there are visual calculation formats for B-spline basis functions as following Fig. 12:

It can be seen from the above relationship that when k> 1, the B-spline basis function of k-order is composed of two B-spline basis functions of order k-1; when k=2, since $B_{i,1}(u)$ is a constant, $B_{i,2}(u)$ is a

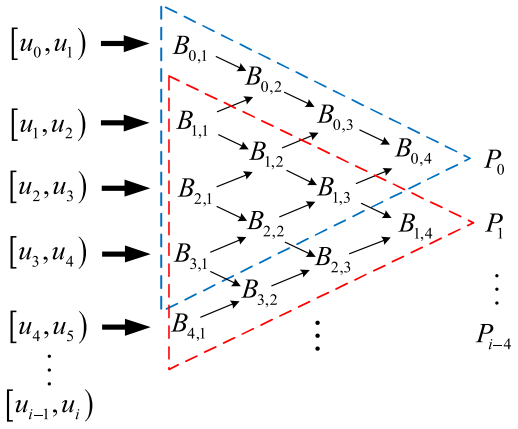

Fig. 12. Recurrence relation of 4-order B-spline basis function.

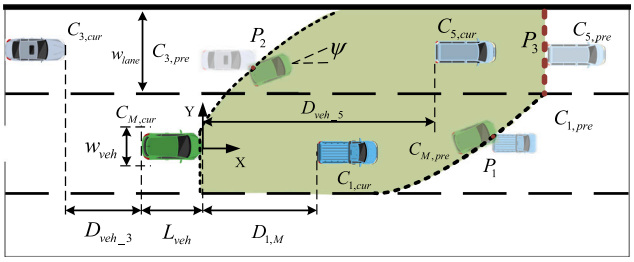

Fig. 13. The relationship between the feasible area and the vehicles.

linear function of u. Therefore, it follows that the k-order B-spline basis function $B_{i,k}(u)$ is a function of degree k-1 with respect to u.

In the planning of lane-changing guide line, vehicles that directly affect the host vehicle include vehicles in front of the current lane, vehicles in front of the target lane, and the target vehicles followed. The feasible area boundary of the host vehicle guide line is limited by the occupied area of surrounding vehicles within the planned step, and the boundary of the driving area is a boundary function changing with time. To obtain the safe feasible area, it is necessary to estimate the motion state of the interacting vehicle and analyze the potential collision between the host vehicle and the others. In order to simplify the analysis process and highlight the algorithm, structured straight roads with clear geometric features are considered and the same geometric size of the vehicles is assumed. The relationship between the feasible area and the vehicles are shown in Fig. 13.

In the figure, *cur* and *pre* in the lower corner mark represent the current position and the future position after a planning step, w_{lane} represents the lane width. w_{veh} represents the width of the vehicle, L_{veh} is the length of the vehicle, ψ is the heading angle of the vehicle, P_i (i=1,2,3) represents the three potential collision boundary points between the host vehicle and the surrounding vehicles.

The green area in the figure indicates the feasible area of lane-changing. In the planning, the position of surrounding vehicles can be predicted by PSO-LSTM trajectory prediction. The coordinates of the three boundary points of potential collision are calculated as follows:

$$\begin{cases} x_{P_1} = \int_0^{t_{C_1}} v_M(t) cos\Psi(t) dt = D_{veh\_1} + \int_0^{t_{C_1}} v_{C_1}(t) dt \\ y_{P_1} = \int_0^{t_{C_1}} v_M(t) sin\Psi(t) dt = \frac{w_{veh}}{2} \end{cases} \tag{21}$$

$$\begin{cases} x_{P_2} = \int_0^{t_{C_3}} v_M(t) cos\Psi(t) dt - L_{veh} cos\Psi_{P_2} \\ \quad = \int_0^{t_{C_3}} v_{C_3}(t) dt - D_{veh\_3} - L_{veh} \\ y_{P_2} = \int_0^{t_3} v_M(t) sin\Psi(t) dt = w_{lane} - \frac{w_{veh}}{2} \end{cases} \tag{22}$$

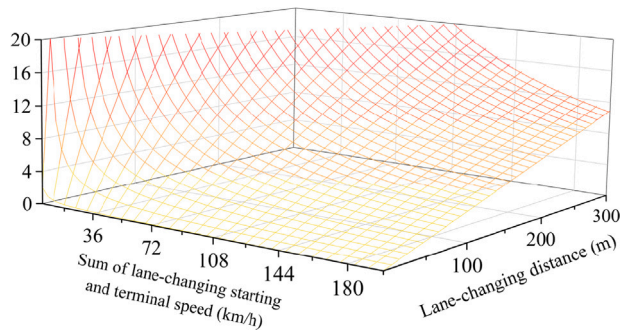

Fig. 14. The relationship of the lane-changing distance, start speed and end speed.

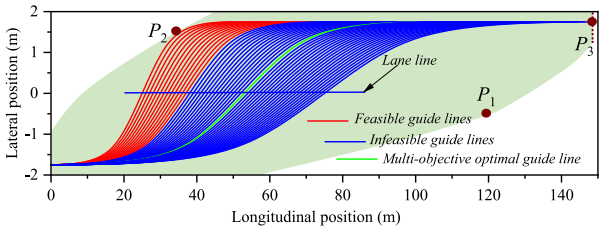

Fig. 15. Lane-changing guide line in feasible area based on B-spline.

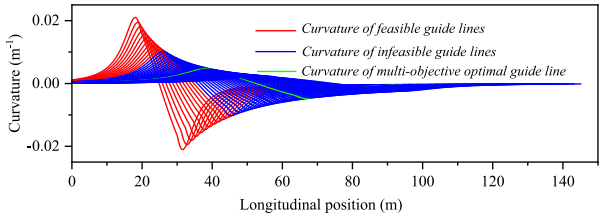

Fig. 16. Curvature for change guide line in feasible area.

$$\begin{cases} x_{P_3} = \int_0^{t_{C_5}} v_M(t)cos\Psi(t)dt = D_{veh_5} + \int_0^{t_{C_5}} v_{C_5}(t)dt \\ y_{P_3} \in [w_{lane}, 2w_{lane}] \end{cases} \tag{23}$$

where x_{P_i} (i=1,2,3) is the horizontal coordinate of the three potential collision points, y_{P_i} (i=1,2,3) is the vertical coordinate of the three potential collision points, $v_M(t)$ is the vehicle speed function of the host vehicle, $v_{C_i}(t)$ represents the vehicle speed of C_i. t_{C_i} is the time of collision with vehicle C_i. The value of t_{C_i} is replaced by the time consumption of completing the lane-changing t_{LC} which can be approximated by the lane-changing distance, starting and terminal speed. The specific relationship is shown in Fig. 14.

The starting position of lane-changing in the feasible area depends on lane-changing decision. The lateral position of the terminal point is the lane center line of the target lane. The longitudinal position is limited by the future position of the vehicle ahead of the target lane after one planned step. In this area, a lane-changing guide line cluster based on B-spline curve is generated as the alternative lane-changing guide lines as shown in Fig. 15. The corresponding curvature obtained by analyzing the guide lines cluster is shown in Fig. 16. According to the movement characteristics of the vehicle, there are the following restrictions: (1) the speed during lane-changing should be less than the critical speed of rollover; (2) different vehicles will have different limit curvature according to the different vehicle structure and steering system performance, the limit curvature of guide line is 0.01 m^{-1}; (3) the sharp change of the front wheel angular speed will directly affect the passenger's comfort; the upper and lower boundaries of the parameters are as follows:

$$|v_M| \le |v_{max}| \tag{24}$$

$$|\omega_M| \le |\omega_{max}| \tag{25}$$

$$|K| \le K_{max} = \frac{1}{\rho_{min}} \tag{26}$$

Among that:

$$v_{max} = \sqrt{\frac{Bg\rho}{2h_s}} \tag{27}$$

$$\rho_{min} = \frac{v_M}{\omega_{max}} \tag{28}$$

$$\omega_{max} = \frac{v_M \delta_{max}}{D_S(1 + K_S v_M^2)} \tag{29}$$

where v_{max} is the maximum speed of the vehicle; K is the curvature of the guide line, K_{max} is the maximum curvature of the guide line, ρ is the curvature radius of the guide line, ρ_{min} is the minimum curvature radius of the guide line, B is the vehicle wheel track, g is the gravitational acceleration, h_s is the height of the vehicle center of gravity from the ground, ω is deflection angular speed of the front wheel, which ω_{max} is the maximum, δ_{max} is the maximum front wheel angle, D_S is the wheelbase of the vehicle, K_s is the stability factor.

The curves that do not meet the restrictions are the infeasible guide line, as the red guide line in Fig. 15. The remaining blue part is the feasible guide line for lane-changing. The extreme value of curvature, average curvature and total length are the main structural parameters of the guide line, so the optimization function is designed as follows:

$$\begin{aligned} \min J_{gui} =& p_{K\_max} cost_{K\_max}^2 \\ &+ p_{K\_mean} cost_{K\_mean}^2 + p_{D\_len} cost_{D\_len}^2 \end{aligned} \tag{30}$$

where $cost_{K\_max}$ is the cost function of extreme curvature, $cost_{K\_mean}$ is the cost function of average curvature, $cost_{D\_len}$ is the cost function of total length, p_{K_max}, p_{K_mean} and p_{D_len} are the weight of the cost function. In order to represent that the three curve evaluation indicators have the same influence and benefit, a fixed weight value is adopted here. To quantify the degree of influence of each cost on the cost function, the extreme value normalization method is adopted to design the cost calculation, as shown below:

$$cost_{K\_max} = max\left\{\frac{K(x_i) - min[K(x)]}{max[K(x)] - min[K(x)]}\right\} \tag{31}$$

$$cost_{K\_mean} = \frac{1}{n_K}\sum_{i=1}^{n_K}\left\{\frac{K(x_i) - min[K(x)]}{max[K(x)] - min[K(x)]}\right\} \tag{32}$$

$$cost_{D\_len} = \frac{D_j - min\left(D_j\right)}{max(D_j) - min\left(D_j\right)} \tag{33}$$

s.t.

$$K(x_i) = \frac{|y_i''|}{\left[1 + (y_i'^2)\right]^{3/2}} \tag{34}$$

$$D_j = \sum_{i=1}^{n_K}\left[\sqrt{\left(x_i - x_{i-1}\right)^2 + \left(y_i - y_{i-1}\right)^2}\right] \tag{35}$$

where x_i and y_i represent the horizontal and vertical coordinates of the discrete point, respectively, $K(x_i)$ is the curvature corresponding to the discrete points of the guide line, i is the number of discrete points, $K(x)$ is the curvature function of each guide line, n_K is the total number of discrete points, and D_j is the length of the guide line.

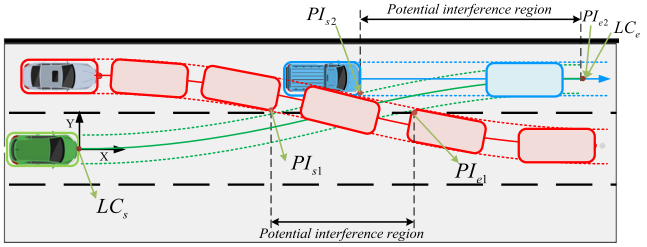

Fig. 17. Potential interference region caused by surrounding vehicle in lane-changing.

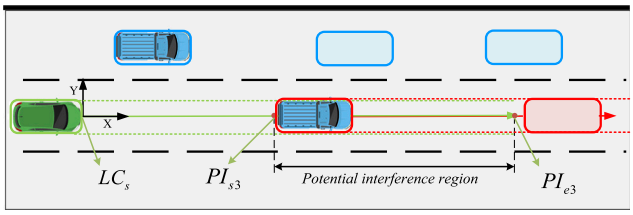

Fig. 18. Potential interference region caused by surrounding vehicle in driving along the center line.

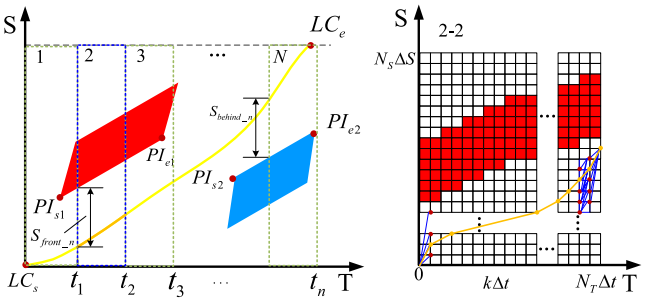

Fig. 19. Speed planning in lane-changing with RDP.

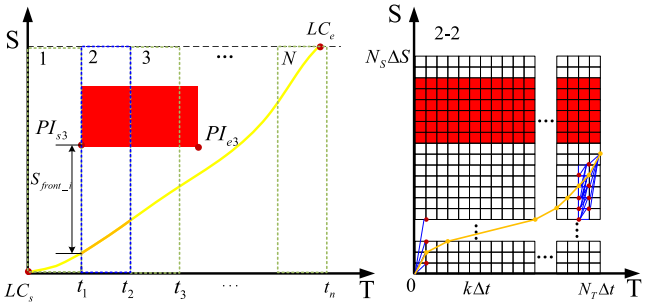

Fig. 20. Speed planning in driving along the center line with RDP.

3.2.2. Energy-efficient speed planning based on RDP

The above guide line planning method provides geometric structure parameters for the vehicle track along the lane center line and lane-changing process. However, surrounding vehicles will impact on the driving of the host vehicle, and the actual speed of the host vehicle is not a simple uniform motion, moreover, random speed allocation for host vehicle is difficult to ensure the safety and economy. Therefore, it is very important to plan the speed when driving along the guide line. The PSO-LSTM network can be used to predict the surrounding vehicles trajectory. The results, as Section 2, show that the accurate prediction can be achieved when the sampling frequency is 25 Hz and the prediction time domain is N_p=25. The trajectory of surrounding vehicles in the future one second can be accurately obtained when the host vehicle speed is planned. With the increase of the prediction time domain, the prediction accuracy will decrease. By analyzing the driving process of the host vehicle, it can be divided into two driving states: driving along the lane-changing guide line and driving along the lane center line as the guide line. When driving along the lane-changing guide line, the driving speed of the host vehicle is affected by the vehicles in the front of the target lane and the vehicles at back of the target lane. For the lane-changing of host vehicle, there is a potential interference region PI_{s1}-PI_{e1} between the future trajectory of vehicles at back of the lane-changing target lane and the guide line of the host vehicle, and another potential interference region PI_{s2}-PI_{e2} is caused by the future trajectory of the vehicle in the front of the lane-changing target lane, as shown in Fig. 17. When driving along the center line of the lane, the guide line of the host vehicle overlaps with the future trajectory of the vehicle in the front of the same lane, and the potential interference region is PI_{s3}-PI_{e3}, as shown in Fig. 18. In order to represent the overlap relationship between the potential interference region and the host vehicle guide line, the ST coordinate system is constructed, which the S represents the coordinates along the guide line from the current position of the host vehicle, and the T represents planning time. Limited by the prediction time domain of trajectory prediction algorithm, it is difficult to directly plan the complete lane-changing process, therefore, which is divided via the time windows (1,2,3... N). In this way, the accuracy of surrounding vehicle trajectory information introduced in each planning process can be guaranteed, which improve the precision of planning. Lane-changing speed planning is shown in Fig. 19, and speed planning for driving along the center line of the lane is shown in Fig. 20. In speed planning, safety is the primary premise, so the distance between the host vehicle and the front-behind are limited by the strong constraints in the planning process.

In Figs. 19 and 20, ΔS is the step size of distance, Δt is the step size of time, N_S is the distance discrete number, N_T is the time discrete number, S_{front_n} and S_{behind_n} are the distance to the vehicles in front and behind at t_n. In the solution process, each searching step k has the following state transition:

$$S_M(k+1) = S_M(k) + \Delta S \tag{36}$$

$$v_M(k+1) = [S_M(k+1) - S_M(k)]/\Delta t \tag{37}$$

$$a_M(k+1) = [v_M(k+1) - v_M(k)]/\Delta t \tag{38}$$

$$j_M(k+1) = [a_M(k+1) - a_M(k)]/\Delta t \tag{39}$$

$$P_M(k+1) = F(N_{mot}(k+1), T_{mot}(k+1)) \tag{40}$$

$$N_{mot}(k+1) = \lambda_{unit}\frac{v_M(k+1) i_g i_0}{r} \tag{41}$$

$$T_{mot}(k+1) = F(a_M(k+1), v_M(k+1)) \tag{42}$$

Constraint by:

$$\begin{cases} S_{front\_n}(k) > \Delta v_f(k) t_{ttc} \\ S_{behind\_n}(k) > \Delta v_b(k) t_{ttc} \\ v_{M\_min} \le v_M(k) \le v_{M\_max} \\ a_{M\_min} \le a_M(k) \le a_{M\_max} \\ j_{M\_min} \le j_M(k) \le j_{M\_max} \\ P_M(k) \le P_{M\_max} \end{cases} \tag{43}$$

where $S_M(k)$ is the driving distance in the time step k, $S_M(k+1)$ is the driving distance in the time step k+1, $v_M(k)$ is the speed in the

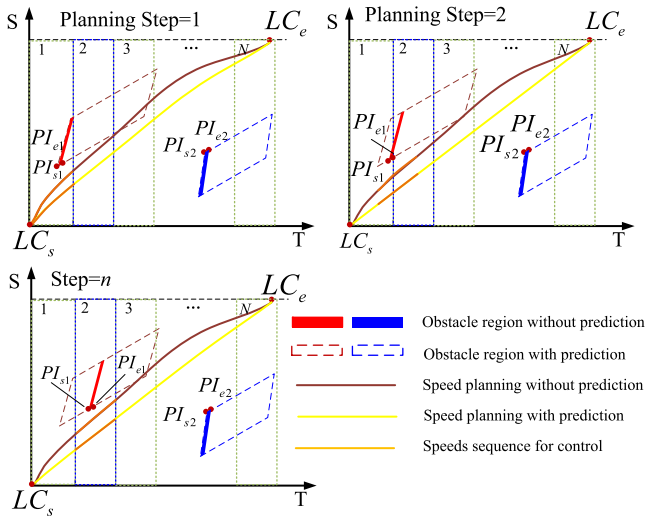

Fig. 21. The vehicle speed planning process when the prediction fails.

time step k, $v_M(k+1)$ is the speed in the time step k+1. $a_M(k)$ is the acceleration in the time step k, $a_M(k+1)$ is the acceleration in the time step k+1, $j_M(k)$ is the jerk in the time step k, $j_M(k+1)$ is the jerk in the time step k+1, $P_M(k+1)$ is the motor power at moment $k+1$, $N_{mot}(k+1)$ and $T_{mot}(k+1)$ are the motor speed and motor torque at moment k+1, $S_{front\_n}(k)$ and $S_{behind\_n}(k)$ are the distance to the vehicles in front and behind in the time step k, $\Delta v_f(k)$ and $\Delta v_b(k)$ are the speed difference with vehicles in front and behind in the time step k, v_{M_min} and v_{M_max} are the maximum and minimum speed of the vehicle, a_{M_min} and v_{M_max} are the maximum and minimum acceleration of the vehicle, and j_{M_min} and j_{M_max} are the maximum and minimum jerk of the vehicle, respectively.

In order to show the performance of the controller when the trajectory prediction information of the surrounding obstacle vehicles is not available. The safety performance of the controller when the predictive function fails is explained. When the prediction fails, only the speed and position information of the current state of obstacle vehicle can be obtained through the sensor and V2V, and the specific presentation in the ST graph is shown as obstacle region without prediction, in Fig. 21. In the planning process, with the update of the planning step, there will be new current obstacle vehicle information obtained, forming a new obstacle region without prediction. At the same time, the new speed curve will be planned. The vehicle speed involved in the control only has the vehicle speed sequence corresponding to a nearby planning step. So, when the prediction algorithm fails, the vehicle will still travel according to the plan. However, because there is no obstacle vehicles prediction sequence to participate in the planning, the energy-efficiency of the planning result will be affected.

In order to improve the calculation rate and real-time performance of algorithm, the motor characteristic data, in Fig. 9, are fitted by polynomial to obtain the relationship between motor power and motor speed and torque, as follows:

$$P_M = \begin{cases} a_{11} + a_{12}N_{mot} + a_{13}T_{mot} + a_{14}N_{mot}^2 \\ +a_{15}N_{mot}T_{mot} + a_{16}T_{mot}^2 \qquad (T_{mot} \geq 0) \\ a_{21} + a_{22}N_{mot} + a_{23}T_m + a_{24}N_{mot}^2 \\ +a_{25}N_{mot}T_m + a_{26}T_{mot}^2 \qquad (T_{mot} < 0) \end{cases} \tag{44}$$

where a_{ij} is energy consumption fitting coefficient of the motor, which i is indicates the working state of the motor (i=1 represents driving state, i=2 represents generating state) and j (j=1,2,3…) is the position of the fitting coefficients in polynomial.

Dynamic programming in each time window is an optimization problem under multiple constraints. In the time window T_i - T_{i+1}, the optimal speed curve satisfies the cost function to ensure the energy-efficiency. The cost function is:

$$minJ_{RDP}(k) = cost_P^2 \tag{45}$$

$$cost_P = \frac{P_M(k) - P_{M\_min}}{P_{M\_max} - P_{M\_min}} \tag{46}$$

where $cost_P$ is the power cost of the vehicle, P_{M_min} is the minimum motor power, and P_{M_max} is the maximum motor power.

In each time window, the result of planned speed is a ST curve composed of multiple ST points. To obtain a smooth ST curve, the curve is smoothed by the quintic polynomial fitting method. In order to ensure the continuity of the smooth curve and avoid too large error from the DP planning result, the optimization function is designed with acceleration, jerk and relative fitting error, and the smoothing equation of the ST curve is as follows:

$$\begin{aligned} minJ_{smo}(k) = &\sum_0^{N_t} \left|a_{fit}(k)\right| + \sum_0^{N_t} \left|j_{fit}(k)\right| \\ &+ \sum_0^{N_t} \left|S_M(k) - S_{fit}(k)\right| \end{aligned} \tag{47}$$

$$\begin{cases} S_{fit}(k) = \frac{1}{120}b_0k^5 + \frac{1}{24}b_1k^4 + \frac{1}{6}b_2k^3 + \frac{1}{2}b_3k^2 + \\ \qquad b_4k + b_5 \\ v_{fit}(k) = \frac{1}{24}b_0k^4 + \frac{1}{6}b_1k^3 + \frac{1}{2}b_2k^2 + b_3k + b_4 \\ a_{fit}(k) = \frac{1}{6}b_0k^3 + \frac{1}{2}b_1k^2 + b_2k + b_3 \\ j_{fit}(k) = \frac{1}{2}b_0k^2 + b_1k + b_2 \end{cases} \tag{48}$$

$$\begin{cases} S_{fit}(0) = S_M(0) \\ v_{fit}(0) = v_M(0) \\ a_{fit}(0) = a_M(0) \\ S_{fit}(N_t) = S_M(N_t) \\ v_{fit}(N_t) = v_M(N_t) \\ a_{fit}(N_t) = a_M(N_t) \\ v_{M\_min} \leq v_{fit}(k) \leq v_{M\_max} \\ a_{M\_min} \leq a_{fit}(k) \leq a_{M\_max} \\ j_{M\_min} \leq j_{fit}(k) \leq j_{M\_max} \end{cases} \tag{49}$$

where $a_{fit}(k)$ is the fitted acceleration, $j_{fit}(k)$ is the fitted jerk, $S_{fit}(k)$ is the fitted driving distance, $v_{fit}(k)$ is the fitted vehicle speed, and b_i (i=0,1,2,3,4,5) is the fitting coefficient of the speed curve, $S_{fit}(0)$ and $S_{fit}(N_t)$ are the fitting start distance and end distance, $v_{fit}(0)$ and $v_{fit}(N_t)$ are the fitting start speed and end speed, and $a_{fit}(0)$ and $a_{fit}(N_t)$ are the fitting start and end acceleration, respectively.

3.3. Weight optimization with model-based

The key parameters are the weight of extreme value of curvature, the weight of average curvature and the weight of total length. By designing the weight assignment standard to test the performance under each case, the weight assignment that meets the performance requirements is optimized. Each weight is divided equally at 0.1 intervals, and the three weights are divided into seven allocation schemes based on different influence degrees. The extreme effect weight distribution scheme is presented as Fig. 22(a), which emphasizes the influence of a single indicator for the guide line optimization function. Fig. 22(b) shows the middle effect weight distribution, which shows that the

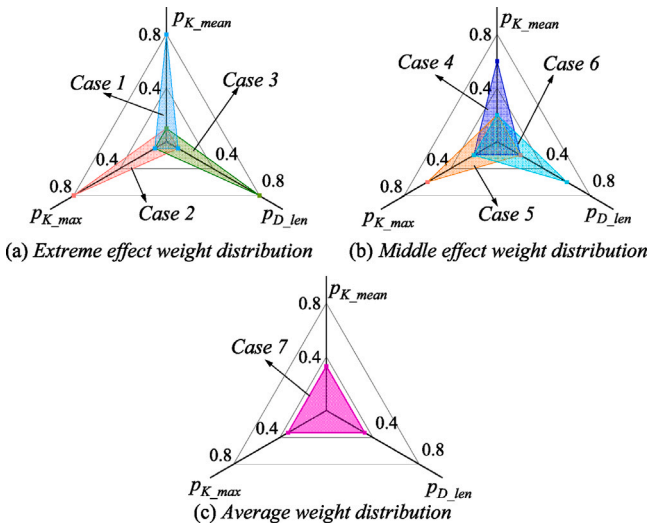

Fig. 22. Weight distribution scheme based on influence degree.

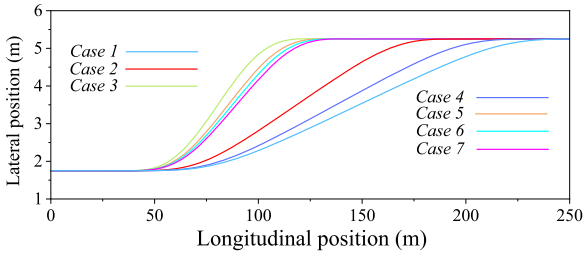

Fig. 23. Lane-changing curves under different weight schemes.

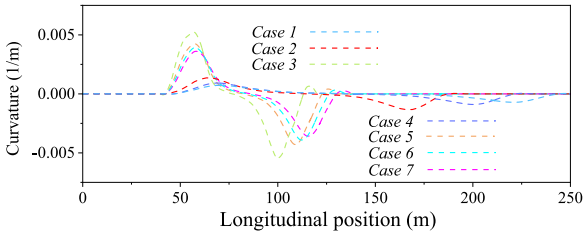

Fig. 24. Curvature of lane-changing curve under different weight schemes.

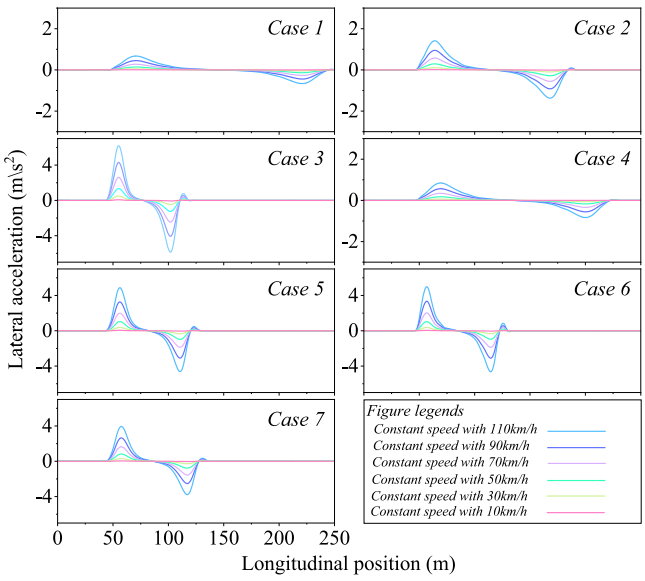

Fig. 25. Lateral acceleration at different speeds.

Table 4
Weight allocation coefficient under typical speed.

Constant speed	Case	P_{K_mean}	P_{K_max}	P_{D_len}
110 km/h	2	0.1	0.8	0.1
90 km/h	5	0.2	0.6	0.2
70 km/h	3	0.1	0.1	0.8
50 km/h	3	0.1	0.1	0.8
30 km/h	3	0.1	0.1	0.8
10 km/h	3	0.1	0.1	0.8

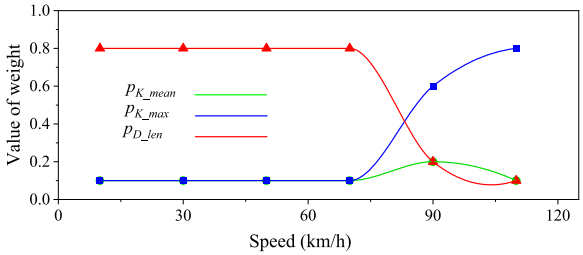

Fig. 26. Weight allocation coefficient curves under all speed conditions.

three indicators are considered apart from extra emphasis on the single indicators. The average weight distribution comprehensively considers three indicators under the same influence in Fig. 22(c). The curves and curvatures of guide lines are shown as Figs. 23 and 24.

It can be seen that the weight allocation affects the geometry and curvature of the lane-changing guide line. The curvature of the curve makes a direct impact on the lateral acceleration of the vehicle during lane-changing. By calculating lateral acceleration of vehicles at different speeds, lateral acceleration under seven weight allocation schemes can be obtained, as shown in Fig. 25.

The extreme value of lateral acceleration in the above schemes is 6.3 m/s^2. In actual driving condition, if passengers are guaranteed to have favorable riding comfort, the lateral acceleration should not exceed 3.5 m/s^2. When the maximum speed is 110 km/h, the lateral acceleration of case 1, case 2 and case 4 meets the comfort requirements, but case 2 has a shorter lane-changing distance. Therefore, the weight allocation of case 2 is selected as the weight coefficient of 110 km/h.

By analogy analysis, the weight coefficients under different speeds are obtained as shown in Table 4, and the weight allocation curves are obtained by connecting typical weight allocation points through the spline curve, as shown in Fig. 26.

4. Trajectory tracking control based on MPC

The task in trajectory tracking control layer is that the trajectory obtained from the above solution (the guide line and the vehicle speed mapped on the guide line constitute the vehicle driving trajectory) is tracked accurately and quickly. As a model-based controller, a suitable vehicle kinematics model is needed to predict the future state of the vehicle driving state. Then, considering the physical constraints of the actuator, the trajectory tracking optimal control problem is proposed. Finally, by solving the proposed optimal control problem in real time, the vehicle speed increment and the front wheel angle increment are obtained (Brüdigam et al., 2021; Ji et al., 2016). In the global

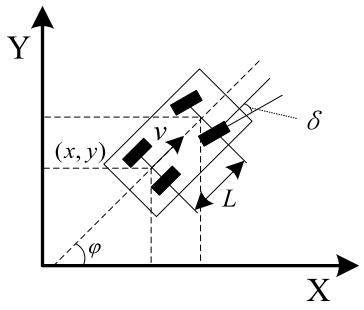

Fig. 27. Schematic diagram of vehicle kinematics model.

coordinate system, the vehicle kinematics equation can be expressed as:

$$\begin{bmatrix}\dot{x}\\ \dot{y}\\ \dot{\varphi}\end{bmatrix}=\begin{bmatrix}\cos\varphi\\ \sin\varphi\\ \frac{\tan\delta}{L}\end{bmatrix}v \tag{50}$$

where $(x,\ y)$ is the center coordinate of the rear axle of the vehicle, φ is the heading angle, and δ is the deflection angle of the front wheel, v is the speed of the center point of the rear axle, and L is the wheelbase, as shown in Fig. 27.

The vehicle kinematics system can be viewed as a control system with inputs $\boldsymbol{u}(v,\delta)$ and state quantities $\chi(x,y,\varphi)$. Based on that, the vehicle trajectory tracking error model is built as follows:

$$\begin{aligned}\dot{\tilde{\chi}}=\begin{bmatrix}\dot{x}-\dot{x}_{ref}\\ \dot{y}-\dot{y}_{ref}\\ \dot{\varphi}-\dot{\varphi}_{ref}\end{bmatrix}&=\begin{bmatrix}0 & 0 & -v_{ref}\sin\varphi_{ref}\\ 0 & 0 & v_{ref}\cos\varphi_{ref}\\ 0 & 0 & 0\end{bmatrix}\begin{bmatrix}x-x_{ref}\\ y-y_{ref}\\ \varphi-\varphi_{ref}\end{bmatrix}\\&+\begin{bmatrix}\cos\varphi_{ref} & 0\\ \sin\varphi_{ref} & 0\\ \frac{\tan\delta_{ref}}{L} & \frac{v_{ref}}{L\cos^2\delta_{ref}}\end{bmatrix}\begin{bmatrix}v-v_{ref}\\ \delta-\delta_{ref}\end{bmatrix}\end{aligned} \tag{51}$$

where $\dot{\tilde{\chi}}$ represents the first derivative of the state quantity deviation, $(x_{ref},y_{ref},\varphi_{ref})$ represents the reference state quantity, and (v_{ref},δ_{ref}) represents the reference input quantity.

In order to further design the model prediction equation, the Eq. (50) is discretized based on the forward Euler method as following:

$$\tilde{\chi}(k+1)=\boldsymbol{A}_{k,t}\tilde{\chi}(k)+\boldsymbol{B}_{k,t}\tilde{\boldsymbol{u}}(k) \tag{52}$$

$$\boldsymbol{A}_{k,t}=\begin{bmatrix}1 & 0 & -v_{ref}\sin\varphi_{ref}T\\ 0 & 1 & v_{ref}\cos\varphi_{ref}T\\ 0 & 0 & 1\end{bmatrix} \tag{53}$$

$$\boldsymbol{B}_{k,t}=\begin{bmatrix}\cos\varphi_{ref}T & 0\\ \sin\varphi_{ref}T & 0\\ \frac{\tan\delta_{ref}T}{L} & \frac{v_{ref}T}{Lcos^2\delta_{ref}}\end{bmatrix} \tag{54}$$

where k represents the discrete time point and T represents the discrete time step. To facilitate further solving the model prediction problem, it is constructed into a quadratic form:

$$\xi(k+1|t)=\tilde{\boldsymbol{A}}_{k,t}\xi(k|t)+\tilde{\boldsymbol{B}}_{k,t}\Delta\boldsymbol{U}(k|t) \tag{55}$$

$$\eta(k|t)=\tilde{\boldsymbol{C}}_{k,t}\xi(k|t) \tag{56}$$

s.t.

$$\xi(k|t)=\begin{bmatrix}\tilde{\chi}(k)\\ \tilde{\boldsymbol{u}}(k-1)\end{bmatrix},\ \tilde{\boldsymbol{A}}_{k,t}=\begin{bmatrix}A_{k,t} & B_{k,t}\\ 0_{m\times n} & I_m\end{bmatrix},\ \tilde{\boldsymbol{B}}_{k,t}=\begin{bmatrix}B_{k,t}\\ I_m\end{bmatrix} \tag{57}$$

where $\tilde{\boldsymbol{C}}_{k,t}$ is coefficient matrix, $\Delta\boldsymbol{U}$ is control input increment, $(k|t)$ indicates to predict the value at k based on the sampled information at t. To improve control efficiency, the hypothesis is proposed: $\boldsymbol{A}_{k,t}=\boldsymbol{A}_{t,t}$, $\boldsymbol{B}_{k,t}=\boldsymbol{B}_{t,t}$, and $\tilde{\boldsymbol{C}}_{k,t}=\tilde{\boldsymbol{C}}_{t,t}$.

The quadratic prediction form of the final prediction equation is:

$$\boldsymbol{Y}(t)=\boldsymbol{\Psi}_t\xi(t|t)+\boldsymbol{\Theta}_t\Delta\boldsymbol{U}(t) \tag{58}$$

$$\boldsymbol{Y}(t)=\begin{bmatrix}\eta(t+1|t)\\ \eta(t+2|t)\\ \cdots\\ \eta(t+N_c|t)\\ \cdots\\ \eta(t+N_p|t)\end{bmatrix} \tag{59}$$

$$\boldsymbol{\Psi}_t=\begin{bmatrix}\tilde{\boldsymbol{C}}_{t,t}\tilde{\boldsymbol{A}}_{t,t}\\ \tilde{\boldsymbol{C}}_{t,t}\tilde{\boldsymbol{A}}_{t,t}^2\\ \cdots\\ \tilde{\boldsymbol{C}}_{t,t}\tilde{\boldsymbol{A}}_{t,t}^{N_c}\\ \cdots\\ \tilde{\boldsymbol{C}}_{t,t}\tilde{\boldsymbol{A}}_{t,t}^{N_p}\end{bmatrix} \tag{60}$$

$$\boldsymbol{\Theta}_t=\begin{bmatrix}\tilde{\boldsymbol{C}}_{t,t}\tilde{\boldsymbol{B}}_{t,t} & 0 & 0 & 0\\ \tilde{\boldsymbol{C}}_{t,t}\tilde{\boldsymbol{A}}_{t,t}\tilde{\boldsymbol{B}}_{t,t} & \tilde{\boldsymbol{C}}_{t,t}\tilde{\boldsymbol{B}}_{t,t} & 0 & 0\\ \cdots & \cdots & \cdots & \cdots\\ \tilde{\boldsymbol{C}}_{t,t}\tilde{\boldsymbol{A}}_{t,t}^{N_C-1}\tilde{\boldsymbol{B}}_{t,t}^{N_C-1} & \tilde{\boldsymbol{C}}_{t,t}\tilde{\boldsymbol{A}}_{t,t}^{N_C-2}\tilde{\boldsymbol{B}}_{t,t} & \cdots & \tilde{\boldsymbol{C}}_{t,t}\tilde{\boldsymbol{A}}_{t,t}^{N_C-4}\tilde{\boldsymbol{B}}_{t,t}\\ \cdots & \cdots & \ddots & \cdots\\ \tilde{\boldsymbol{C}}_{t,t}\tilde{\boldsymbol{A}}_{t,t}^{N_p-1}\tilde{\boldsymbol{B}}_{t,t} & \tilde{\boldsymbol{C}}_{t,t}\tilde{\boldsymbol{A}}_{t,t}^{N_p-2}\tilde{\boldsymbol{B}}_{t,t} & \cdots & \tilde{\boldsymbol{C}}_{t,t}\tilde{\boldsymbol{A}}_{t,t}^{N_p-N_c-1}\tilde{\boldsymbol{B}}_{t,t}\end{bmatrix} \tag{61}$$

$$\boldsymbol{U}(t)=\begin{bmatrix}\Delta\boldsymbol{u}(t|t)\\ \Delta\boldsymbol{u}(t+1|t)\\ \cdots\\ \Delta\boldsymbol{u}(t+N_c|t)\end{bmatrix} \tag{62}$$

In the discrete vehicle model system, it is necessary to add optimization function according to the control objective to ensure the performance of the controller. To optimize the tracking of the controller, the optimization objective function based on the quadratic form of the prediction equation is constructed as follows:

$$\begin{aligned}min\boldsymbol{J}_{smo}(k)=&\sum_{i=1}^{N_p}\left\|\boldsymbol{\eta}(k+i|t)-\boldsymbol{\eta}_{ref}(k+i|t)\right\|_Q^2\\&+\sum_{i=1}^{N_c-1}\|\Delta\boldsymbol{U}(k+i|t)\|_R^2+\rho\varepsilon^2\end{aligned} \tag{63}$$

where Q and R are the weight matrix of the output item and control increment item respectively, and $\rho\varepsilon^2$ is the relaxation factor term to prevent the solving process from no solution. The control quantity and control increment are constrained. In the objective function, the variable to be solved is the control increment in the control time domain. The form of constraints is as follows:

$$\Delta\boldsymbol{U}_{min}\le\Delta\boldsymbol{U}(t)\le\Delta\boldsymbol{U}_{max} \tag{64}$$

$$\boldsymbol{U}_{min}\le\boldsymbol{U}(t)+\boldsymbol{A}\Delta\boldsymbol{U}(t)\le\boldsymbol{U}_{max} \tag{65}$$

$$\boldsymbol{U}(t)=\boldsymbol{1}_{N_c}\boldsymbol{u}(k-1),k=0,1,2,\ldots,N_c-1 \tag{66}$$

$$\Delta\boldsymbol{U}(t)=\begin{bmatrix}\Delta\boldsymbol{u}(t|t)\\ \Delta\boldsymbol{u}(t+1|t)\\ \cdots\\ \Delta\boldsymbol{u}(t+N_c|t)\end{bmatrix} \tag{67}$$

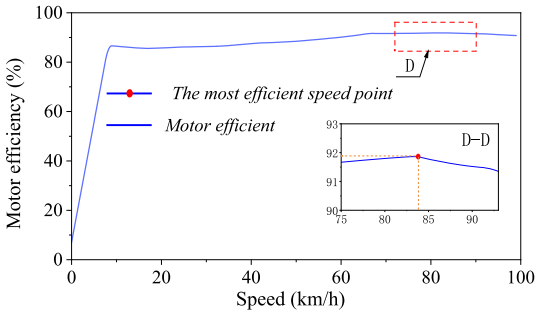

Fig. 28. The relationship between stable speed and motor efficiency.

$$\boldsymbol{A} = \begin{bmatrix} 1 & \cdots & 0 & 0 \\ 1 & 1 & \cdots & 0 \\ \vdots & \vdots & \ddots & \vdots \\ 1 & 1 & \cdots & 1 \end{bmatrix} \otimes I_m \tag{68}$$

where $\Delta \boldsymbol{U}(t)$ is the control increment sequence in the prediction time domain, $\boldsymbol{U}(t)$ is the actual control quantity sequence in the prediction time domain, $\mathbf{1}_{N_c}$ is the column vector with the number of rows N_c, I_m is the identity matrix with dimension m, $\otimes$ is the Kronecker product, and $\boldsymbol{u}(k-1)$ is the actual control quantity at the last time.

5. Results and discussion

This section will verify the effectiveness and superiority of the algorithm, which the verification process is based on the HiL. The research objective is to improve the energy-efficient performance of EVs in the planning and control process. Firstly, the energy flow of vehicles is analyzed. The energy transfer efficiency of vehicles during driving mainly consists of three parts: mechanical efficiency (gear box efficiency, final drive efficiency), motor efficiency and battery efficiency. The mechanical efficiency and battery efficiency cannot be directly changed by vehicle planning and control, while the motor efficiency is directly related to the driving state of the vehicle. In order to obtain the relationship between motor efficiency and vehicle driving state, full-condition test was carried out. As shown in Fig. 28, motor efficiency corresponding to the stable speed from 0 km/h to 100 km/h was traversed to characterize the energy conversion efficiency of the vehicle. The most efficient speed point is 83.7 km/h, corresponding to the motor efficiency of 91.7%.

The configuration of HiL mainly includes three parts: algorithm run layer, EV test platform and scene establishment. The EV test platform is equipped with vehicle-mounted controller and vehicle dynamic model to represent the actual motion process of the EVs. The actual state of the EV and its position in the scene are transmitted to the algorithm run layer in real time for planning and control at the next moment. The configuration of HiL test platform is as Fig. 29.

In order to further reflect the superiority of the algorithm, this part firstly makes a comparative analysis with the energy-efficient solution in the existing literature and the planning method that does not consider energy-efficient in the planning. Among the energy-efficient solutions in the existing literature are economic adaptive cruise control (EACC) (Pan et al., 2022). The energy-efficient performance will be tested on the full 600 m urban condition and 1000 m expressway condition.

According to Figs. 30 and 31, EACC makes different decisions when it encounters an obstacle vehicle compared with our proposed method, EACC chooses to follow the obstacle vehicle, while our proposed method makes a lane-changing decision to achieve the more energy-efficient speed state, which are shown in Fig. 32. The overall comparison of energy consumption under two conditions shows that

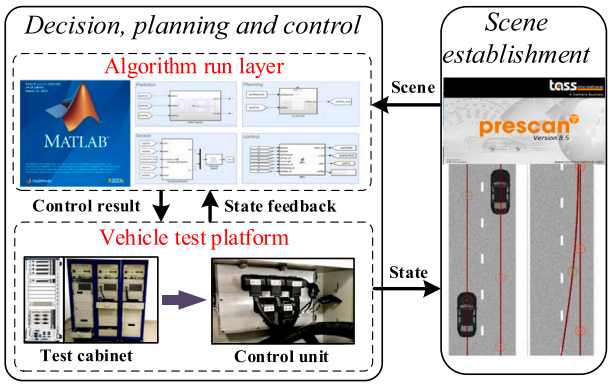

Fig. 29. The configuration of HiL test platform.

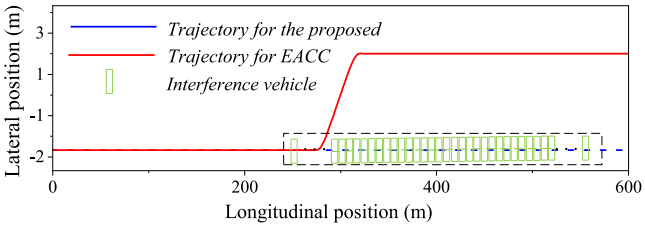

Fig. 30. Driving trajectory under urban condition between EACC and the proposed.

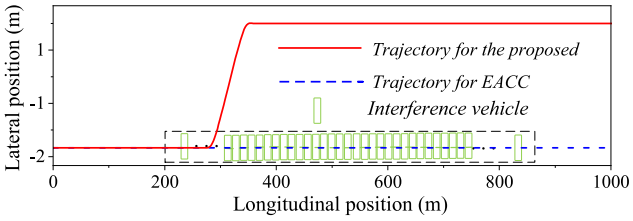

Fig. 31. Driving trajectory under expressway condition between EACC and the proposed.

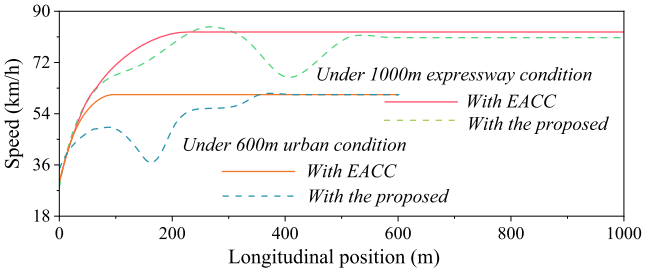

Fig. 32. Speed under urban and expressway condition with EACC and the proposed.

our proposed method has better performance in energy efficiency, as Fig. 33. Next, the detailed validation of the algorithm effectiveness and superiority under different operating conditions is carried out.

5.1. Testing for the algorithm verification under urban condition

In the urban condition, according to the relevant standards of China's national road structure, the two-lane scene with one-way driving is selected for road structure, and the speed limit of the two-lane is 60 km/h. In a 600 m long test scene, the actual motion information of surrounding vehicles within a certain period of time is collected to build a test environment. The vehicle performance was tested under

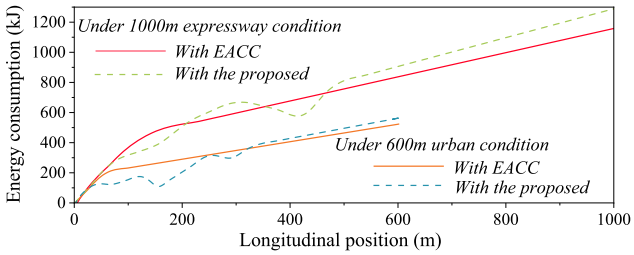

Fig. 33. Energy consumption under urban and expressway condition with EACC and the proposed.

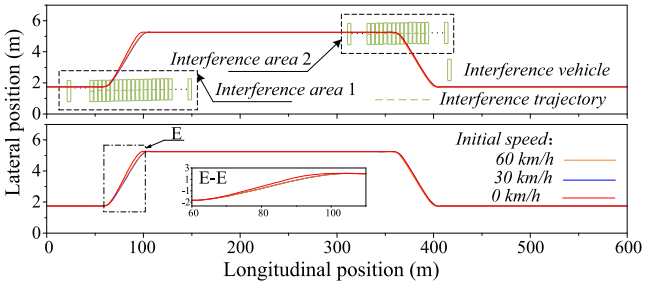

Fig. 34. Driving trajectory under urban condition.

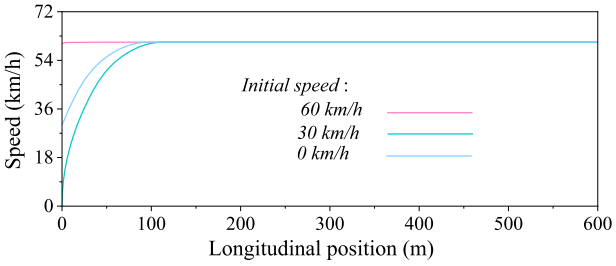

Fig. 35. Speed for the driving trajectory under urban condition.

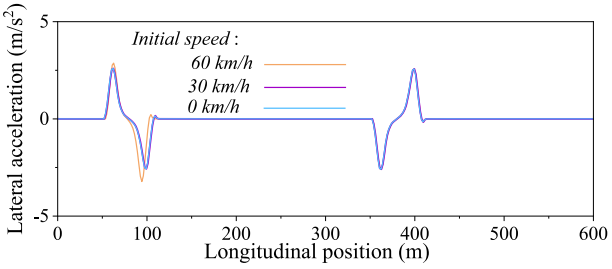

Fig. 36. Lateral acceleration for the driving trajectory under urban condition.

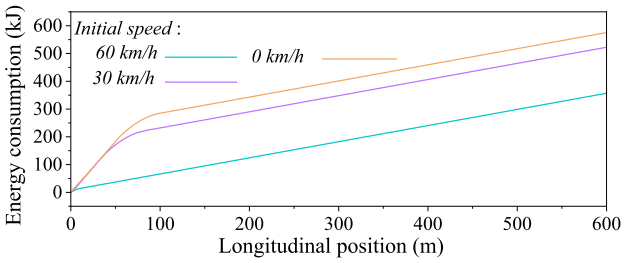

Fig. 37. Energy consumption for the driving trajectory under urban condition.

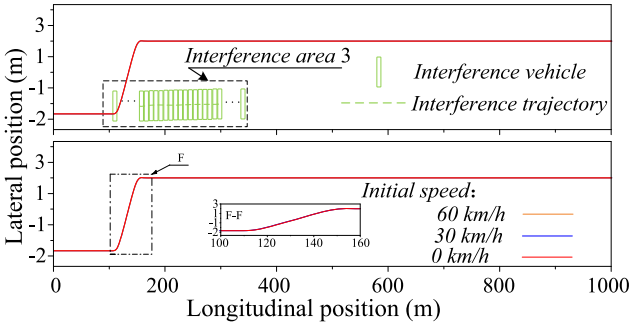

Fig. 38. Driving trajectory under expressway condition.

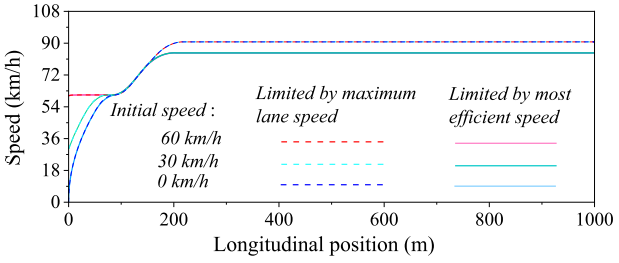

Fig. 39. Driving trajectory under expressway condition.

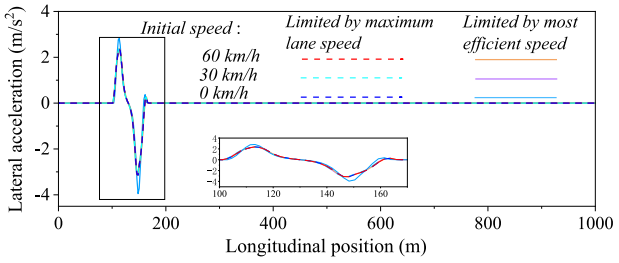

Fig. 40. Lateral acceleration for the driving trajectory under expressway condition.

different initial speed respectively, and the test results are shown as Figs. 34–37.

As can be seen from Fig. 34, in the interference area 1 at the initial stage, due to the interference vehicle with speed lower than that of host vehicle in the same lane, the decision-making result of the host vehicle is lane-changing if the main vehicle wants to achieve an energy-efficient speed as soon as possible under the premise of the road speed limit. As the similar condition for the interference area 2, the host vehicle decides to change lane. In Fig. 35, the maximum vehicle speed is 60 km/h. Combined with Fig. 28, under the urban condition speed limit, the motor efficiency corresponding to 60 km/h is the highest. As can be seen from Fig. 36, the maximum lateral acceleration of the vehicle in two lane-changes is less than 2.5m/s^2, which meets the comfort requirements of passengers. Fig. 37 shows the energy consumption for different initial speeds, reflecting that the energy consumption increase rate of the vehicle during acceleration is higher than that during constant speed driving.

5.2. Testing for the algorithm verification under expressway condition

Figs. 38 and 39 shows that the lane-changing occurs when the vehicle is in the interference area 3. The results indicate that the vehicle changes lanes from the lane with speed limit of 60 km/h to the lane with speed limit of 90 km/h. In that lane-changing, the vehicle seeks higher energy-efficiency potential under the premise of ensuring safe driving, since the most efficient speed of the host vehicle is 83.7 km/h. Fig. 40 shows that the lateral acceleration caused by lane-changing is

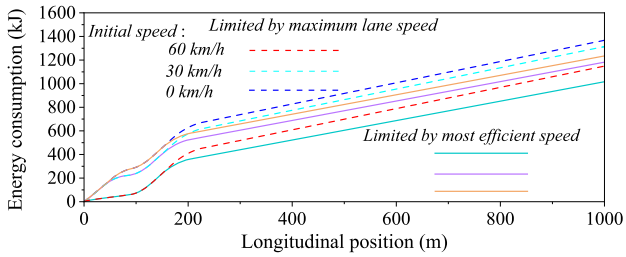

Fig. 41. Energy consumption for the driving trajectory under expressway condition.

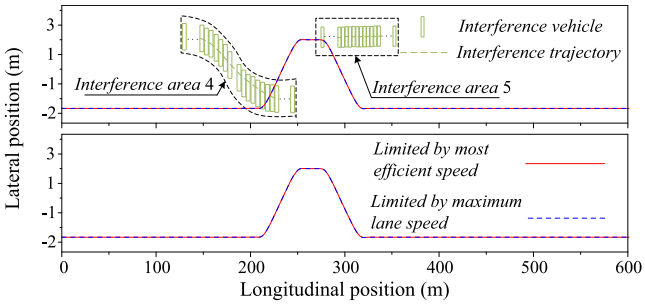

Fig. 42. Driving trajectory under sudden condition of the urban area.

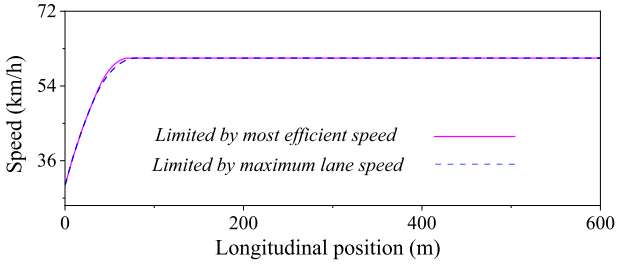

Fig. 43. Speed for driving trajectory under sudden condition of the urban area.

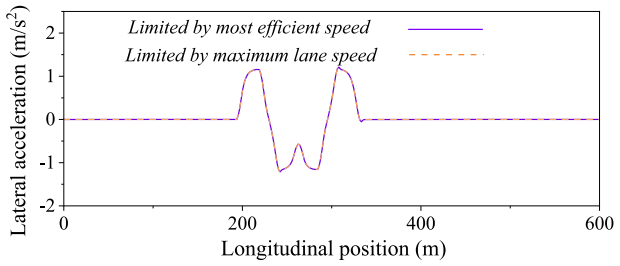

Fig. 44. Lateral acceleration for driving trajectory under sudden condition of the urban area.

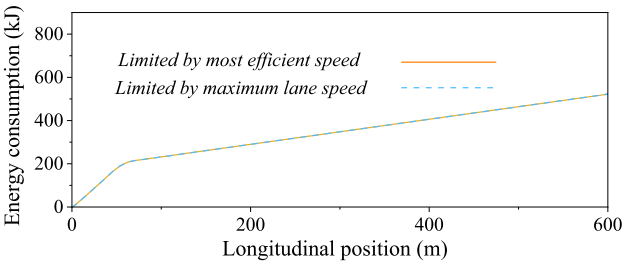

Fig. 45. Energy consumption for driving trajectory under sudden condition of the urban area.

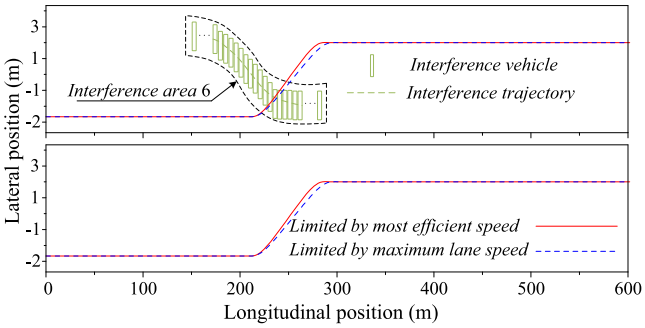

Fig. 46. Driving trajectory under sudden condition of the expressway.

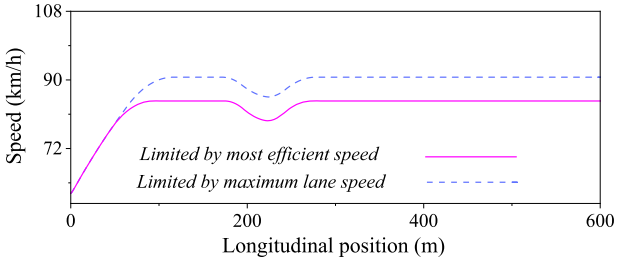

Fig. 47. Speed for driving trajectory under sudden condition of the expressway.

also the same due to the same planned trajectory and the vehicle speed under the two speed limit constraints. When changing to the lane with speed limit of 90 km/h, the speed planning result under the energy-efficiency constraint is the most efficient speed as shown in Fig. 39. Comparing the two speed limit constraints, the planning result limited by the most efficient speed has better energy saving performance as shown in Fig. 41.

5.3. Testing for the algorithm verification under sudden condition

This subsection respectively verifies the effectiveness of the planning of the algorithm for the sudden conditions, which the vehicle in the side lane cuts in the current lane of the host vehicle under the urban condition and the expressway condition. The verification results are shown in Figs. 42–49.

As can be seen from Fig. 42, 43 and 44, when the vehicle drives to interference area 4, the vehicle changes lane for the first time in order to ensure the safety and economy of driving. In this case, the vehicle speed is 60 km/h, which is the highest efficient vehicle speed under the speed limit of the urban condition. When the vehicle drives to interference area 5, it changes lane for the second time due to the influence of the current vehicle in front, so as to ensure the safety. At the same time, in order to pursue economy, the speed is kept at 60 km/h. The maximum lateral acceleration of this process is less than $2/s^2$. In urban conditions, the lane speed limit is equal to the most efficient speed in urban areas, therefore, the energy consumption performance is the same under the two speed limits. However, under this plan, vehicles can pass through this road section at a higher speed, which improves the traffic efficiency to some extent. Since the two cases have the same vehicle speed trajectory, the energy consumption is the same in Fig. 45.

As can be seen from Fig. 46, 47 and 48, when the vehicle drives to interference area 6, the vehicle changes lane. Affected by the inserted vehicle, the host vehicle performs a speed planning process of first slowing down and then accelerating to ensure safety. When driving in the lane with 90 km/h speed limit, compared two speed limits, host vehicle driving at the constraint with most efficient speed passes

Table 5
Analysis of the proposed algorithm test results.

Conditions	Method	Consumption (kJ)			Improving rate (%)		
		Initial speed			Initial speed		
		0 km	30 km	30 km	0 km	30 km	60 km
Urban condition	A	575.46	523.26	356.88	0	0	0
	B	575.46	523.26	356.88			
Expressway condition	A	1368.56	1315.23	1149.86	9.68	10.07	11.56
	B	1236.10	1182.77	1017.38			
Urban sudden condition	A	\	523.26	\	\	0	\
	B	\	523.26	\			
Expressway sudden condition	A	\	\	820.04	\	\	13.14
	B	\	\	712.26			

* Method A is the proposed without considering for energy-efficiency, and method B is the proposed.

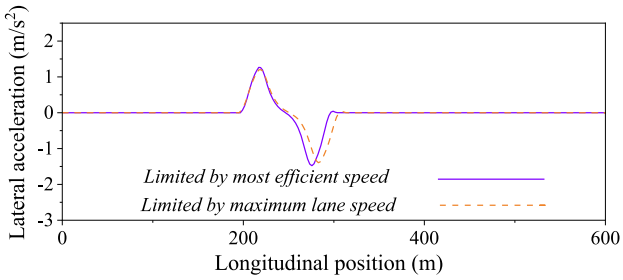

Fig. 48. Lateral acceleration for driving trajectory under sudden condition of the expressway.

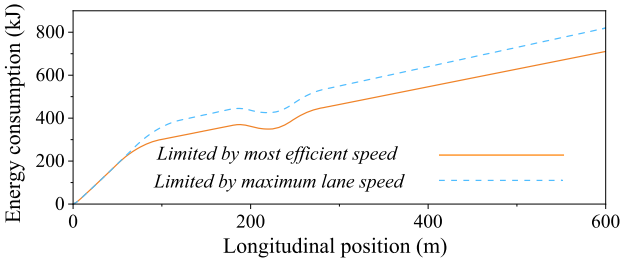

Fig. 49. Energy consumption for driving trajectory under sudden condition of the expressway.

through this road which has better energy saving performance, as Fig. 49.

Comprehensive analysis of the performance in urban area and expressway shows that the vehicle in expressway has higher energy saving potential, since the most efficient speed for this test vehicle is 83.7 km/h. Therefore, on the premise of ensuring driving safety, the vehicle should be driven at a higher speed to pursue the energy-efficiency.

6. Conclusion

In this paper, an energy-efficient trajectory planning with curve splicing based on PSO-LSTM trajectory prediction is proposed. It is composed of energy-efficient trajectory planning layer and trajectory tracking control layer, and the method was tested under urban and expressway conditions, and the results are shown in Table 5. The detailed research conclusions are as follows:

1. To express the impact of surrounding vehicle trajectory on the planning, this study used LSTM network to model the trajectory prediction. To improve the accuracy of the model by adjusting the hyperparameters, the PSO algorithm was adopted to dynamically optimize the hyperparameters. The results showed that, compared with the conventional LSTM, the PSO-LSTM had higher prediction accuracy under the same data-drive.

2. For the decision-making of energy-efficient trajectory planning, the vehicle longitudinal dynamic equation based on motor MAP was used to construct the correlation between vehicle driving energy consumption and motor efficiency. The energy-efficient decision function was designed by the average efficiency and target behavior efficiency in the process of behavior switching.

3. The trajectory planning process was divided into two steps. The B-spline curve adopted to plan the guide line for behavior switching, and the RDP was utilized to plan the energy-efficient speed. To improve the adaptability of the curve splicing, the weight optimization scheme based on condition traversal was designed, which constructed the weight allocation curve of all working conditions by selecting the optimal weight value under typical working conditions

4. In order to ensure the tracking ability of the vehicle to the energy-efficient trajectory, the tracking control method based on MPC was designed, which took the vehicle speed and the front wheel angle as the control variables and the reference trajectory as the target.

The final test results show that the energy-efficient effect of the algorithm application is obvious in the expressway condition. When the initial speed of EV is different, the energy consumption improving rate of the planning algorithm considering energy-efficiency is different, and the average energy consumption improving rate is 11.11%.

The method designed in this paper optimized the economy of the existing trajectory planning research and improved the energy-saving performance of the vehicle driving process. In the future, the algorithm will be verified on the real vehicle to realize the practical application of the algorithm.

CRediT authorship contribution statement

Jian Wang: Writing – original draft, Software, Formal analysis, Data curation. **Zhongxing Li:** Supervision, Investigation. **Chaofeng Pan:** Resources, Project administration, Investigation, Funding acquisition.

Declaration of competing interest

No conflict of interest exits in the submission of this manuscript, and manuscript is approved by all authors for publication. I would like to declare on behalf of my co-authors that the work described was original research that has not been published previously, and not under consideration for publication elsewhere in whole or in part. All the authors listed have approved the manuscript that is enclose and they have contributed hard-working to the research.

Acknowledgments

This research was funded by the National Natural Science Foundation of China, grant number [52272367].

References

Abousleiman, R., & Rawashdeh, O. (2015). Energy consumption model of an electric vehicle. In *2015 IEEE transportation electrification conference and expo* (pp. 1–5). IEEE, http://dx.doi.org/10.1109/ITEC.2015.7165773.

Brüdigam, T., Olbrich, M., Wollherr, D., & Leibold, M. (2021). Stochastic model predictive control with a safety guarantee for automated driving. *IEEE Transactions on Intelligent Vehicles*, *8*(1), 22–36. http://dx.doi.org/10.1109/TIV.2021.3074645.

Chalaki, B., & Malikopoulos, A. A. (2021). Optimal control of connected and automated vehicles at multiple adjacent intersections. *IEEE Transactions on Control Systems Technology*, *30*(3), 972–984. http://dx.doi.org/10.1109/TCST.2021.3082306.

Chen, Y., Hu, C., & Wang, J. (2019). Motion planning with velocity prediction and composite nonlinear feedback tracking control for lane-change strategy of autonomous vehicles. *IEEE Transactions on Intelligent Vehicles*, *5*(1), 63–74. http://dx.doi.org/10.1109/TIV.2019.2955366.

Dibaei, M., Zheng, X., Jiang, K., Abbas, R., Liu, S., Zhang, Y., Xiang, Y., & Yu, S. (2020). Attacks and defences on intelligent connected vehicles: A survey. *Digital Communications and Networks*, *6*(4), 399–421. http://dx.doi.org/10.1016/j.dcan.2020.04.007.

Fiori, C., Ahn, K., & Rakha, H. A. (2016). Power-based electric vehicle energy consumption model: Model development and validation. *Applied Energy*, *168*, 257–268. http://dx.doi.org/10.1016/j.apenergy.2016.01.097.

He, H., Wang, Y., Han, R., Han, M., Bai, Y., & Liu, Q. (2021). An improved MPC-based energy management strategy for hybrid vehicles using V2V and V2I communications. *Energy*, *225*, Article 120273. http://dx.doi.org/10.1016/j.energy.2021.120273.

Huang, Y., Du, J., Yang, Z., Zhou, Z., Zhang, L., & Chen, H. (2022). A survey on trajectory-prediction methods for autonomous driving. *IEEE Transactions on Intelligent Vehicles*, *7*(3), 652–674. http://dx.doi.org/10.1109/TIV.2022.3167103.

Ji, J., Khajepour, A., Melek, W. W., & Huang, Y. (2016). Path planning and tracking for vehicle collision avoidance based on model predictive control with multiconstraints. *IEEE Transactions on Vehicular Technology*, *66*(2), 952–964. http://dx.doi.org/10.1109/TVT.2016.2555853.

Krajewski, R., Bock, J., Kloeker, L., & Eckstein, L. (2018). The highd dataset: A drone dataset of naturalistic vehicle trajectories on german highways for validation of highly automated driving systems. In *2018 21st international conference on intelligent transportation systems* (pp. 2118–2125). IEEE, http://dx.doi.org/10.1109/ITSC.2018.8569552.

Li, H., Wu, C., Chu, D., Lu, L., & Cheng, K. (2021). Combined trajectory planning and tracking for autonomous vehicle considering driving styles. *IEEE Access*, *9*, 9453–9463. http://dx.doi.org/10.1109/ACCESS.2021.3050005.

Liang, H., Li, H., Gao, J., Cui, R., & Xu, D. (2022). Economic MPC-based planning for marine vehicles: Tuning safety and energy efficiency. *IEEE Transactions on Industrial Electronics*, *70*(10), 10546–10556. http://dx.doi.org/10.1109/TIE.2022.3220876.

Lin, Q., Li, S. E., Xu, S., Du, X., Yang, D., & Li, K. (2020). Eco-driving operation of connected vehicle with V2I communication among multiple signalized intersections. *IEEE Intelligent Transportation Systems Magazine*, *13*(1), 107–119. http://dx.doi.org/10.1109/MITS.2020.3014113.

Liu, Y., Zhou, B., Wang, X., Li, L., Cheng, S., Chen, Z., Li, G., & Zhang, L. (2021). Dynamic lane-changing trajectory planning for autonomous vehicles based on discrete global trajectory. *IEEE Transactions on Intelligent Transportation Systems*, *23*(7), 8513–8527. http://dx.doi.org/10.1109/TITS.2021.3083541.

Luin, B., Petelin, S., & Al-Mansour, F. (2019). Microsimulation of electric vehicle energy consumption. *Energy*, *174*, 24–32. http://dx.doi.org/10.1016/j.energy.2019.02.034.

Ma, F., Yang, Y., Wang, J., Li, X., Wu, G., Zhao, Y., Wu, L., Aksun-Guvenc, B., & Guvenc, L. (2021). Eco-driving-based cooperative adaptive cruise control of connected vehicles platoon at signalized intersections. *Transportation Research Part D: Transport and Environment*, *92*, Article 102746. http://dx.doi.org/10.1016/j.trd.2021.102746.

Manzinger, S., Pek, C., & Althoff, M. (2020). Using reachable sets for trajectory planning of automated vehicles. *IEEE Transactions on Intelligent Vehicles*, *6*(2), 232–248. http://dx.doi.org/10.1109/TIV.2020.3017342.

Min, H., Xiong, X., Yang, F., Sun, W., Yu, Y., & Wang, P. (2023). An energy-efficient driving method for connected and automated vehicles based on reinforcement learning. *Machines*, *11*(2), 168. http://dx.doi.org/10.3390/machines11020168.

Miri, I., Fotouhi, A., & Ewin, N. (2021). Electric vehicle energy consumption modelling and estimation—A case study. *International Journal of Energy Research*, *45*(1), 501–520. http://dx.doi.org/10.1109/TITS.2019.2961705.

Nie, Z., & Farzaneh, H. (2023). Energy-efficient lane-change motion planning for personalized autonomous driving. *Applied Energy*, *338*, Article 120926. http://dx.doi.org/10.1016/j.apenergy.2023.120926.

Pan, C., Huang, A., Wang, J., Chen, L., Liang, J., Zhou, W., Wang, L., & Yang, J. (2022). Energy-optimal adaptive cruise control strategy for electric vehicles based on model predictive control. *Energy*, *241*, Article 122793. http://dx.doi.org/10.1016/j.energy.2021.122793.

Rahman, M., Chowdhury, M., Xie, Y., & He, Y. (2013). Review of microscopic lane-changing models and future research opportunities. *IEEE Transactions on Intelligent Transportation Systems*, *14*(4), 1942–1956. http://dx.doi.org/10.1109/TITS.2013.2272074.

Shieh, S.-Y., Ersal, T., & Peng, H. (2023). Pulse-and-glide operations for hybrid electric vehicles in the car-following scenario. *IEEE Transactions on Vehicular Technology*, http://dx.doi.org/10.1109/TVT.2023.3260021.

Sun, C., Guanetti, J., Borrelli, F., & Moura, S. J. (2020). Optimal eco-driving control of connected and autonomous vehicles through signalized intersections. *IEEE Internet of Things Journal*, *7*(5), 3759–3773. http://dx.doi.org/10.1109/JIOT.2020.2968120.

Tian, Z., Liu, L., & Shi, W. (2021). A pulse-and-glide-driven adaptive cruise control system for electric vehicle. *International Transactions on Electrical Energy Systems*, *31*(11), Article e13054. http://dx.doi.org/10.1002/2050-7038.13054.

Wang, H., Lu, B., Li, J., Liu, T., Xing, Y., Lv, C., Cao, D., Li, J., Zhang, J., & Hashemi, E. (2021). Risk assessment and mitigation in local path planning for autonomous vehicles with LSTM based predictive model. *IEEE Transactions on Automation Science and Engineering*, *19*(4), 2738–2749. http://dx.doi.org/10.1109/TASE.2021.3075773.

Wang, Y., Wang, L., Guo, J., Papamichail, I., Papageorgiou, M., Wang, F.-Y., Bertini, R., Hua, W., & Yang, Q. (2022). Ego-efficient lane changes of connected and automated vehicles with impacts on traffic flow. *Transportation Research Part C: Emerging Technologies*, *138*, Article 103478. http://dx.doi.org/10.1016/j.trc.2021.103478.

Wang, Y., & Wei, C. (2020). A universal trajectory planning method for automated lane-changing and overtaking maneuvers. *Mathematical Problems in Engineering*, *2020*(1), Article 1023975. http://dx.doi.org/10.1155/2020/1023975.

Weißmann, A., Görges, D., & Lin, X. (2018). Energy-optimal adaptive cruise control combining model predictive control and dynamic programming. *Control Engineering Practice*, *72*, 125–137. http://dx.doi.org/10.1016/j.conengprac.2017.12.001.

Werling, M., Ziegler, J., Kammel, S., & Thrun, S. (2010). Optimal trajectory generation for dynamic street scenarios in a frenet frame. In *2010 IEEE international conference on robotics and automation* (pp. 987–993). IEEE, http://dx.doi.org/10.1109/ROBOT.2010.5509799.

Xie, D.-F., Fang, Z.-Z., Jia, B., & He, Z. (2019). A data-driven lane-changing model based on deep learning. *Transportation Research Part C: Emerging Technologies*, *106*, 41–60. http://dx.doi.org/10.1016/j.trc.2019.07.002.

Yao, Z., Deng, H., Wu, Y., Zhao, B., Li, G., & Jiang, Y. (2023). Optimal lane-changing trajectory planning for autonomous vehicles considering energy consumption. *Expert Systems with Applications*, *225*, Article 120133. http://dx.doi.org/10.1016/j.eswa.2023.120133.

Ye, F., Hao, P., Qi, X., Wu, G., Boriboonsomsin, K., & Barth, M. J. (2018). Prediction-based eco-approach and departure at signalized intersections with speed forecasting on preceding vehicles. *IEEE Transactions on Intelligent Transportation Systems*, *20*(4), 1378–1389. http://dx.doi.org/10.1109/TITS.2018.2856809.

Zhang, L., Zhu, Z., Zhang, Z., Song, G., Zhai, Z., & Yu, L. (2022). An improved method for evaluating eco-driving behavior based-on speed-specific vehicle-specific power distributions. *Transportation Research Part D: Transport and Environment*, *113*, Article 103476. http://dx.doi.org/10.1016/j.trd.2022.103476.

Zhao, X., Ye, Y., Ma, J., Shi, P., & Chen, H. (2020). Construction of electric vehicle driving cycle for studying electric vehicle energy consumption and equivalent emissions. *Environmental Science and Pollution Research*, *27*, 37395–37409. http://dx.doi.org/10.1007/s11356-020-09094-4.

Zhuang, W., Qu, L., Xu, S., Li, B., Chen, N., & Yin, G. (2020). Integrated energy-oriented cruising control of electric vehicle on highway with varying slopes considering battery aging. *Science China Technological Sciences*, *63*(1), 155–165. http://dx.doi.org/10.1007/s11431-019-9559-2.